Delft University of Technology

Master thesis

All-solid-state batteries: The interface between Li-metal and the solid state electrolyte Li_6PS_5Cl

---

Supervisor: Dr. ir. M. Wagemaker, Dr. S. Ganapathy
Author: Eveline van der Maas
Student number: 4626575
Date: 15.07.2018

Abstract

Lithium ion batteries are currently the most attractive choice for mobile energy storage and power sources [4] in terms of energy density. However, it is unlikely that current battery chemistries will reach the energy density desired for future applications [8]. Li-metal, which has the highest reduction potential of all metals and the highest achievable capacity per weight unit, could significantly increase the energy density when used as an Anode. Unfortunately, the dendritic growth of Li-metal is a safety hazard, and the low electrochemical potential of Li-metal is outside the stability window of many electrolytes leading to capacity degradation.

It has been suggested that safe Li-metal Anodes may be possible in combination with solid electrolytes, as the higher shear modulo of solid over liquid electrolytes may be able to suppress dendrite formation [21].
To study the stability of the interface between Li-metal and the solid electrolyte Li_6PS_5Cl, electrochemical measurements of the cells, ex-situ x-ray diffraction, and solid state Nuclear Magnetic Resonance measurements were made. It was not possible to confirm the decomposition products that were proposed in literature by density functional theory calculations and in-situ XPS. The XRD-pattern of the cycled electrolyte did not show additional phases. The NMR spectra developed broader peaks and one additional phosphorous environment upon cycling.

As a tool to study dendritic growth through Li-ion concentration profiles, a cell for in-situ neutron depth profiling (NDP) was developed. The electrochemical performance is comparable to regular cells, except for a voltage drop due to contact problems during the break after Li-metal stripping. A thin layer of Li-metal between the window and the electrolyte pellet, as well as a collimator plate to put some pressure on the window, could be the solution to go towards operando measurements.

The current standard data analysis method was implemented and its sensitivity towards gaussian broadening, due to energy straggling (from small angle scattering in the material and the stochastic nature of energy loss), was investigated. It is shown that the standard deviation of energy straggling is larger than that of energy broadening due to the detector resolution, and that the error on the depth scale is in the order of micrometers.

Preface

In the beginning of September, 2017, I started with my master thesis project at the reactor institute at Delft university of technology in the group Sustainable Electrochemical Energy storage SEE. With many barbecues, climbing, sailing, and skiing, I was happy to be in probably the most socially active group of the university. Now, upon completion of my thesis, I look back on a great time with nice people and new friendships.

The last 11 months, I got the chance to work on very interesting topics and areas in battery science. Among them solid-state electrolytes, Li-metal anodes, many experimental challenges and a variety of measurement methods. With a very broad topic and almost endless possibilities, it took me a long time to figure out the exact scope of my thesis. I would like to thank all the many people who were available for interesting discussions, and who helped me both with theory and in the labs.

Special thanks go to my daily supervisor Swapna Ganapathy. I always felt very independent while working on my thesis, and you always encouraged me to follow my own ideas and interests. Still, whenever I needed help or advice, I knew I could rely on your great expertise. I learned a lot from you.

I would further like to thank Frans Ooms, for collaborating with me during the cell development, for all the great ideas, and the general support.

My gratitude also goes to Michel Steenvoorden, for the support with the neutron depth profiling setup, and Tomas Verhallen, for giving valuable inputs that lead to some of the key-points in this thesis.

Eveline van der Maas Delft, July 2018

Contents

List of Figures

List of Tables

1. Introduction

Lithium ion batteries are, thanks to their high energy density and long cycle life, currently the most attractive choice for mobile energy storage and power sources [4]. Lithium ion battery packs have an energy density of around 80-150 Wh/kg [28, 33]. The energy density has been increasing at a rate of 7-8% per year, but that will come to an end as the batteries approach the practical energy density limit of the current Lithium ion chemistries [7]. It is unlikely that these will manage to reach energy density targets required for the desired mileage in all electric cars or operation time of mobile IT devices [8]. It has, therefore, been widely accepted that new battery chemistries need to be developed to reach the energy demand for such applications [17].
One approach to increase the energy density of Li-ion batteries is to use Li-metal as Anode, which has the highest reduction potential of all metals and the highest achievable capacity per unit weight. The idea is not new; the first rechargeable lithium power source was a Li-metal cell with a MoS_2 cathode, which was commercialized by Moli Energy in the 1980s. However, the cells had to be recalled due to frequent accidents stemming from various issues, one of which was fires caused by dendrite formation [17, 24]. Other companies like NEC and Mitsui intensively tested the reliability of the cells, but the further development of Li-metal cells was suppressed by the successful introduction of the rocking chair Li-ion battery [17] with $LiCoO_2/LiC_6$ by Sony in 1991, which was aimed at powering mobile phones and was superior in terms of reliability and well suited for large scale production [24]. Since then, many advancements have been made concerning investigative tools and nanotechnology-based solutions [17]. These new possibilities, in combination with the demand for higher energy density batteries, have put the Li-metal anode back into focus for many researchers.

One possibly safe approach for batteries with Li-metal Anodes is the use of solid electrolytes.The higher shear modulo of solid over liquid electrolytes may be able to suppress dendrite formation [21], which would significantly improve the reliability of the cells. Other advantages include a larger range of operating temperatures due to the lower risk of leaks and flammability [1], the avoidance of gas build-up of the liquid electrolyte [37] and, according to many researchers, higher practical energy and power densities can be reached [14, 39].
Still, the introduction of solid electrolytes poses fundamental challenges. A great deal of research has been devoted to finding electrolyte materials with high conductivity. For a solid electrolyte to compete with the performance of standard liquid electrolytes, bulk conductivity of 10^{-2} to $^{-3}$ is required. To date, several electrolytes have been reported with conductivities in this range. It has recently been shown that transport across the solid-solid interface can be several orders of magnitudes lower compared to bulk diffusion [41]. In addition to good transport properties, the interface should be electrochemically stable, or form a self-limited, passivating, interphase with sufficient Li-ion conductivity and negligible electronic conductivity. If this is not the case, the battery will suffer from low coulombic efficiency, increasing internal impedance, or decreasing power capabilities.

For batteries with Lithium metal Anodes and solid electrolytes, many interfacial properties are a challenge to assess experimentally. Generally, many processes in batteries have a transient, non-equilibrium nature. Therefore, it is expected that in-situ diagnostic techniques will play a critical role for performance characterizations [12]. In-situ arises from the Latin "on site" meaning that the battery can be measured without disassembly, enabling measurements in-between cycling. The related term ex-situ, in comparison, means that the battery disassembled before the measurement. The problem with in-situ measurements is that relaxation mechanisms can lead to loss of information [26]. In such cases, operando measurements, which means measuring while the battery is cycling, can lead to meaningful insights.

The purpose of this thesis is to study the interface between Lithium metal and the solid-state electrolyte Li_6PS_5Cl for all solid-state, high energy density batteries. The main focus is the development of a new electrochemical cell which can be used for in-situ and (in the near future) operando neutron depth profiling (NDP). NDP is a non-destructive measurement method which can be used to probe Li-ion concentrations up to around 40 micrometers inside a material. Such measurements can provide meaningful insights in processes like dendritic growth orthogonal to the current collector or a growing interphase, due to the higher Li-concentration of the decomposition products. Also relaxation mechanisms may be studied, by monitoring the concentration profile right after turning off the battery.
Due to the different aspects that may influence the Li-ion concentrations, prior knowledge about the electrochemical system is necessary to interpret NDP spectras. Therefore, batteries are assembled and cycled under different conditions to gain knowledge about the cycling performance. Furthermore, a literature study has been performed and ex-situ x-ray diffraction (XRD) and Solid state nuclear magnetic resonance (NMR) measurements have been made in an attempt to confirm decomposition products that have been either identified or proposed in literature.

The structure of this thesis is as follows: In the remainder of this chapter, first some basic theory about solid electrolytes, Li-metal Anodes and interfaces is outlined. Literature on the electrolyte Li_6PS_5CL, the interface it forms with Li-metal, and Li-metal Anodes is discussed in more detail. Further, the main measurement methods, Neutron depth profiling (NDP), x-ray diffraction (XRD) and solid-state nuclear magnetic resonance (NMR), are introduced.
In the second chapter "Material and Methods", first the scope of the thesis is outlined quickly. Then, experimental details about the material synthesis, the cell preparation measurement details are reported. In the third chapter "Results", the measurement results are shown, the NDP cell development is documented and thoughts about the NDP-data analysis are elaborated. In the Final chapters, "Discussion" and "Conclusion and Recommendations", the findings are discussed, and future research ideas are proposed.

1.1 All-solid-state Li-metal batteries

In this section, the relevant theoretical background is outlined and previous research is introduced. First, basic theory about the diffusion mechanism in solid electrolytes and the interface between two solids is briefly outlined. The properties of the electrolyte Li_6PS_5Cl are summarized. The factors which make Li-metal an ideal Anode for Li-based batteries are discussed in addition to some of the related problems. The dendritic growth mechanism of Lithium metal during electroplating is studied in more detail with an emphasis on why solid electrolytes are often proposed as a possible solution. Finally, literature about the interface between Li_6PS_5Cl and Li-metal is

summarized.

1.1.1 Solid-state Electrolytes

Diffusion in solid electrolytes

Diffusion can be defined by a particle flux which is driven by a concentration or chemical potential difference and is described by Fick's first law of diffusion.

$$j = -D\nabla C \tag{1.1}$$

with j as the current density, D the diffusion coefficient and ∇C the concentration gradient. In a solid material, diffusion results from a hopping process of the diffusing atoms between different lattice sites. There are two main diffusion coefficients that are defined. The first one is related to the hopping frequency Γ

$$D = \frac{1}{d}a^2\Gamma \tag{1.2}$$

where *d* is the dimensionality of the diffusion process and *a* the jump distance. This coefficient describes the total amount of ionic movements between different sites and can be measured experimentally using relaxation NMR. For a jump to occur, an energy barrier has to be overcome. A flat potential energy landscape is therefore characteristic for good ionic conductors. Diffusion described as above does not give information about the distance a specific ion moves relative to a point of origin, which is described by the tracer diffusion coefficient

$$D = \frac{\langle x^2 \rangle}{2\tau} \tag{1.3}$$

where $\langle x^2 \rangle$ is the mean squared net displacement during the time τ. As the total displacement can be viewed as a sum of individual jumps, the two diffusion coefficients can be related by a correlation factor which indicated the amount of back and forth jumps between sites. Diffusion coefficients often show Arrhenius behavior which describes the variation in temperature [18]

$$D = gf\upsilon^0 a^2 exp\left(-\frac{\Delta H}{k_B T}\right) exp\left(\frac{\Delta S}{k_B}\right) = D_0 exp\left(-\frac{\Delta H}{k_B T}\right) \tag{1.4}$$

where *g* is a geometrical factor, *f* the correlation factor, υ^0 the attempt frequency, and *a* the jump distance between the lattice sites. The diffusion coefficient is related to the conductivity by the Nernst-Einstein relation [14]

$$\sigma = \frac{ne^2z^2D}{kT} \tag{1.5}$$

where *n* is the particle density, *e* the electronic charge, *z* the amount of ionic charge, *D* the diffusion coefficient, *k* the Boltzmann coefficient, and *T* the temperature.

The solid electrolyte - electrode interface

Unlike the energy spectrum of a free particle , that of solid materials is not continuous, but is quantized and depends on the local arrangement of the atoms. In metals, these energy levels are very close to each other, generally smaller than $3k_bT$, which allows the transport of electrons. In semiconductors or insulators, there are regions where there are no allowed energy levels known as the band gap. To ensure that no there is no electron transport through the electrolyte, the electrolyte should have a band gap that covers the potential range of the

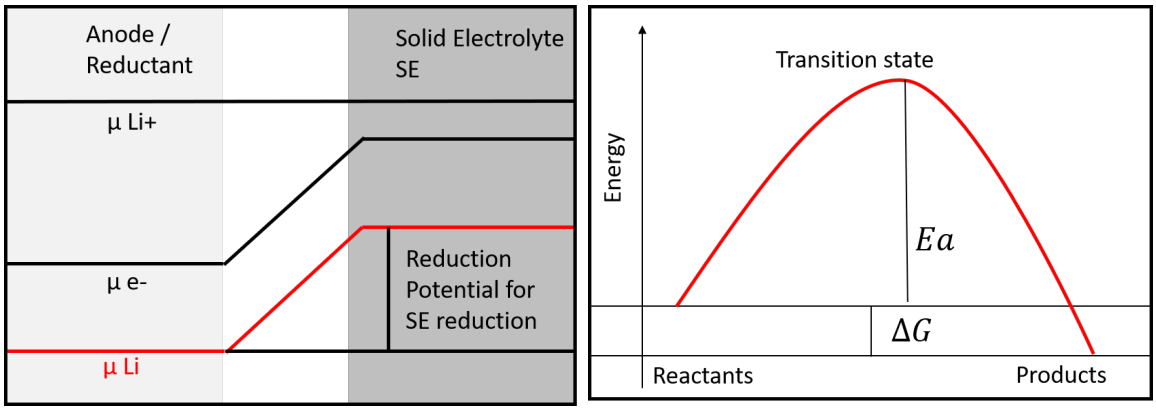

Figure 1.1: Left: Schematic of the energy levels between a solid electrolyte and an Anode separated by an interphase. Image redrawn according to [45]. Right: schematic illustration of the Energy landscape for the charge transfer reaction at the interface.

electrodes during the operation of the battery.
As both the electrode and electrolyte conduct Li-ions, it can be assumed that the energy level of Li-ions is flat. As electrons (ideally) can not be transported in the electrolyte, the energy level of the electrons across the interface does not equilibrate. This translates to a chemical potential gradient between the electrode and electrolyte phases, as illustrated for Li-metal in Figure 1.1. If the electrolyte phase is at higher potential than the electrode phase there is a driving force for the reduction (when considering the Anode side) of the electrolyte. If the kinetics allow, this will lead to the formation of an interphase.
The interface between the electrode and the electrolyte serves as a reaction center for the oxidation/reduction reactions during the operation of the battery. During discharge, there is a thermodynamic driving force for the Lithium to go into the electrolyte, however, there is a energy barrier, the activation energy, that needs to be overcome for the reaction to proceed (Figure 1.1). The current density across the interface can be written as

$$i_{interface} = zFckexp\left(-\frac{\Delta G_A}{RT}\right) \tag{1.6}$$

where c is the ion concentration, F the Faraday constant and ΔG_A the activation energy. Subtracting the cathodic from the anodic current density, and introduction of the applied overpotential, leads to the well-known Butler Volmer equation:

$$i = i_A - i_c = i_0\left(exp\left(\frac{(1-\alpha)zF\eta}{RT}\right) - exp\left(\frac{\alpha zF\eta}{RT}\right)\right) \tag{1.7}$$

where η is the applied overpotential, α the activity, z the ionic charge and i_o the exchange current density. Butler Volmer kinetics assume that the Li-ion transfer is the limiting factor, which is accurate in most cases. It has been shown that in specific cases, the electron transfer at the interface can also be rate limiting, in which case Marcus theory should be applied [2].

Requirements for Solid Electrolytes

In batteries or electrochemical cells, the role of the electrolyte is to transport the ions between the electrodes while blocking the electrons. When looking for new electrolyte candidates, one has to be aware of the requirements they need to fulfill their role and to be practically applicable. For solid-state electrolytes, following attributes have been named [37]:

1. High ionic bulk conductivity at ambient and sub-ambient temperature
2. Low interfacial and or grain boundary resistance
3. Good electronic insulator
4. Thermal and electrochemical stability
5. Li_+ transference number close to one
6. Good mechanical strength
7. Compatibility with electrodes
8. Environmentally friendly

High ionic bulk conductivity ensures efficient operation and allows practical power densities. Conductivity is always a function of temperature and should be optimized for the usual working condition of the device. At lower temperature, charge transfer kinetics and Li-ion conductivity are lower, so the internal impedance of the battery is higher. The battery, therefore, operates less efficiently and can provide less power. In current Li-ion cells, the energy output reduces to 60 % when the temperature drops from 25 degrees to -20, a substantial energy loss. The higher charging overpotential can also lead to Li-plating on the graphite anode during charging, which accelerates aging of the battery [13]. In current electric cars, this problem is often avoided by heating the battery, which also requires a vast amount of energy; a practice which emphasizes the importance of battery performance, sans environmental control, in a wide range of operating temperatures.
Low interfacial conductivity is related to the charge transfer reaction and the transport of lithium ions to the electrolyte and electrons through the electrode. When the energy barrier for those processes is high, kinetics will generally be low and can be the rate limiting process of the battery. The same accounts for the **grain boundary resistance**.
The electrolyte has to be a **good electronic insulator** in order to avoid internal transport of electrons and therewith to minimize self-discharge. However, a more convenient measure than electronic insulation is the **transference number**:

$$t_i = \frac{\sigma_i}{\sigma_i + \sigma_e} \tag{1.8}$$

as electronic self discharge will be low, if the electronic transport is much slower compared to the ionic, which relates to a transference number close to 1.
Mechanical strength is needed because the solid electrolyte should ideally replace both the liquid electrolyte and the separator. Therefore, the solid electrolyte should also serve as a physical barrier between the electrodes.
Compatibility with electrodes is determined by several aspects. First of all, the band gap of the electrolyte has to be in the right position relative to the energy level of the electrode materials, to avoid harmful side reactions and the degradation of the battery. Then, as described above, the transport between electrode and electrolyte has to be efficient, so charge transfer should have a low energy barrier and the materials should form good mechanical contact.
Finally, the materials used should be **environmentally friendly**. Considering that, for example, the weight of the battery of a Tesla Model S (2017) is 580 kg (with 150.9 Wh/kg), it is clear that the materials should be abundant and accessible. Additionally, new chemistries will have to be economically competitive with current lithium ion batteries, which means materials have to be cheap, all production processes have to be scalable, and, ideally, at low temperatures .

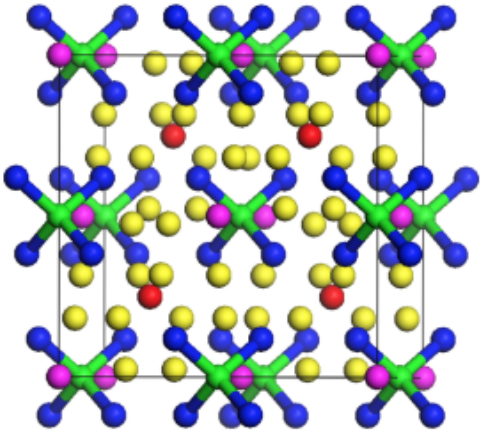

Figure 1.2: The crystal structure of the high temperature phase of $Li_7 7S_6$. The 48h Lithium sites are drawn in yellow, the phosphorous green, sulfur sites bound to phosphorous blue, sulfur 4a sites pink and 4c sites red. Figure reused from [14].

Li_6PS_5Cl

Li_6PS_5Cl is part of the sulphide electrolytes, more specifically of the Lithium Argyrodites. The structure and conduction process have been simulated by Molecular Dynamics (MD) simulations with density functional theory (DFT) in [14], a brief summary is given here.

The Lithium Argyrodites can be characterized by the general Formula Li_7PnCh_6, where Pn is either P or As and Ch can be replaced O, S or Se. Li_6PnCh_5X can be obtained by replacing one Ch by a halogen (X). In Figure 1.2, one unit cell for the high temperature phase of Li_7PS_6 is shown. To obtain Li_6PS_5Cl, the Chloride substitutes Sulfur 4a or 4c sites. Of the 48h Lithium sites, around 50% are occupied. The 4c sulfur sites are surrounded by six pairs (12 in total) 48h Lithium sites, which form a cage like structure.
Three different kinds of jumps have been identified within the lattice structure. The first consists of jumps between the pairs of Lithium sites over a distance of 1.9 Angstrom (doublet jumps), the second is jumps within the cage of 2.25 angstrom (intra cage jump) and the third jumps interconnecting the cages (inter cage jump), with varying jump distances. The MD simulations have shown whether or not jumps are rate limiting depends on the chloride site occupancy. When all Chlorides are located on 4a sites, the intercage jumps are limiting. When all occupy the 4c sites, the doublet jump is rate limiting. The optimal Chloride distribution to maximize conductivity is 1:3 over 4a and 4c sites.
In [41], the conductivity of Li_6PS_5Cl was further investigated with a combination of impedance measurements, MD-simulations and ^{7}Li solid-state NMR experiments. The NMR measurements showed two different motional processes in the argyrodite, which were attributed to jumps around the Cl and S positions within the cagelike structure and inter cage transitions. These findings were in good agreement with the MD-simulations. The comparison with impedance spectroscopy indicated a large positive influence of the grain boundaries on the overall conductivity.
The electronic conductivity is 5 orders of magnitude lower than the ionic conduction, which means that Li_6PS_5Cl is almost a pure ionic conductor [44].
In [45] DFT studies were performed to investigate the electrochemical stability of different solid electrolytes. For Li_6PS_5Cl a very narrow stability window was calculated with a reduction potential of 1.7 V and a oxidation potential of 2.01 V (vs. Li/Li^+). The phase equilibrium at the reduction potential consists of LiCl, Li_2S and

elemental Phosphorous. At the oxidation potential it formed Li_3PS_4, LiCl and elemental Sulfur.
The chemical stability of the electrolyte is a important factor for the design and choice of experimental setups and could greatly influence the complexity of production processes. Generally, Argyrodites are very reactive when exposed to water. For Argyrodites, the following reaction with H_2O has been proposed from DFT calculations [5]]:

$$Li_{7-x}PS_{6-x}X_x + (8-2x)H_2O <-> LiX + Li_3PO_4 + (6-x)H_2S + (4-2x)LiOH \tag{1.9}$$

In [44], the influence of 24h exposure to air on the conductivity of the electrolyte has been tested and found to be relatively small. However, the degradation mechanism and the influence on other properties were not studied.

1.1.2 Li-metal Anodes

In this section, firstly a brief discourse on the attractiveness, and difficulties, associated with the use of Li-metal anodes is presented. Then, the growth mechanism of Li-metal during electroplating is elaborated, different theoretical growth models are outlined, and the reason why solid electrolytes are thought to suppress dendrites is treated. Finally, previous research done for Li-metal Anodes with the Electrolyte Li_6PS_5Cl is summarized.

The benefits and problems of Li-metal Anodes

The voltage V of a battery is defined as the difference in potential Φ between the Cathode and the Anode:

$$V = \Phi_{Cathode} - \Phi_{Anode} \tag{1.10}$$

When voltage and capacity C of a battery is known, the theoretical energy density E_d can be calculated by:

$$E_d \left[\frac{J}{kg}\right] = \frac{V * C}{M} \tag{1.11}$$

s
where M is the mass of the electrodes. A good Anode for high energy density batteries should therefore have a high capacity per unit weight and low electrochemical potential. Considering the low weight of Lithium and that (theoretically) no host material is needed, it is clear that the capacity per unit weight is maximized. Further more, lithium metal has the most negative standard electrode potential among all metals [11]. Numerically, Li-metal has a theoretical capacity of 3860 mAh/g (or 2.061 mAh/cm^-3) and -3.04 V compared to the standard hydrogen electrode [17]. These properties make Lithium metal the ideal Anode for high-energy-density batteries. However, several problems present themselves when using Li-metal as Anode:

- Due to the low electrochemical potential, Li-metal falls out of the voltage window of many known electrolytes. This can lead to oxidation of the electrolyte at the interface, leading to the formation of an interphase. This leads to low coulombic efficiency, electrolyte consumption, or, when the decomposition products have very high ionic resistance, can even lead to impedance failure of the battery.
- The volume change upon Lithium plating is very large (3mAh/cm^3 corresponds to a thickness of 14.6 um Li-metal [17]). This can lead to large stresses on the interface. This is problematic for SEI stability in liquid electrolyte batteries and physical/mechanical contact in solid electrolyte batteries.
- Lithium does not form a homogeneous metal layer when plating. Various forms have been reported such as pillar-like, mossy, needle-like, whisker and dendritic structures, which depends on the substrate, the

electrolyte materials, and current density. The formation of dendrites is a critical problem, as it can lead to large capacity degradation because of dead Lithium (electronically insulated Lithium metal pieces in the electrolyte), or internal short-circuit when they penetrate the separator which is a severe safety issue. When Lithium grows in the form of dendrites, the surface area exposed to the electrolyte also becomes significantly larger, which can lead to enhanced electrolyte decomposition.

For these reasons, dendritic growth can be considered one of the main problems for Li-metal Anodes and is therefore discussed in more detail below.

Dendritic growth mechanism of Lithium metal

The mechanisms behind Li deposition have been studied extensively, as evidenced by the vast amount of review articles. The main focus of these articles varies, including topics like fundamental chemical aspects such as nucleation, growth mechanisms and morphologies [7], experimental methods to study the growth mechanisms [43], methods to suppress dendritic growth [17], and different quantitative growth models [16]. The full discussion of all these factors are out of the scope of this thesis. Here, the quantitative models are introduced briefly according to [16], as they are useful for illustrating why solid electrolytes may suppress dendrite formation.

There are three main models that have been used to describe the electro deposition of metals on a electrode surface:

- **Surface tension model**
  The surface tension model was initially developed for silver plating in liquid electrolytes. It assumes that new ions are preferentially deposited at the dendrite tip or a surface irregularity, due to the larger spherical diffusion rate compared to a flat surface. At a certain dendrite thickness, the surface tension does not allow further thinning, leading to an equilibrium thickness. The model divides between two current density regimes: At low current density the dendrite growth rate is proportional to the overpotential η. At high current density the dendrite growth rate is proportional to η^2.

- **Brownian statistical model**
  In the Brownian statistical model a simulation domain is defined that contains an active region and some randomly distributed active sites. Dissolved ions are randomly distributed within the whole domain. When an ion hits one of the active sites or the active region, there is a certain probability that the ion will be deposited on the site. This probability depends on the overpotential, the limiting current, the exchange current density, and the bulk electrolyte concentration. With a low deposition probability, the diffusion dominates and Lithium ions can diffuse deeper inside the structure leading to a denser deposition. Under a high deposition probability, the contrary happens and the deposition is favored at the tips of the structure. The extreme case of diffusion-limited growth assumes a deposition probability of 1, which corresponds to Sand's well known model [30].

- **Chazalviel electromigration limited model**
  The Chazaviel model was initially developed for a system of two copper electrodes immersed in aqueous $CuSO_4$ electrolyte. It was found that the regions near the positive electrode was depleted from anions when

a large voltage was applied (around 10 Volts), and a positive space charge region formed that initiated the dendrite growth from the root of the dendrite on the electrode surface. The growth rate was found to be a function of the anionic mobility and proportional to the local current density.

Due to high current densities, the Chazaviel model is not relevant for processes in Li-ion batteries [16].
The surface tension model was further applied to Li/polymer systems under galvanostatic conditions [19]. In a follow up study, the effect of elasticity, viscous drag and mechanical pressure was added to the model to describe the kinetics of roughening interfaces [20]. The model was further applied to solid electrolytes and it was found that interfacial roughening, which is the initial stage of dendrite formation, was mechanically suppressed when the separator shear modulus is about twice that of Li-metal [21]. The shear modulus of Li-metal is 4.2 GPa, which means that electrolytes with a shear modulus higher 8.4 GPa should suppress dendrite formation.

For example, the shear modulus of Li_2S-P_2S_5 (cold) hot pressed pellets was measured to be (14-17) 18-25 GPa [29], which should be enough to suppress dendrite formation. However, in [23], for example, Lithium metal deposition was studied with a electrolyte consisting of $80Li_2S$-$20P_2S_5$ with in-situ SEM (scanning electron microscopy). It was found that at current densities higher than $1mA/cm^2$, the Li grew along grain boundaries inside the electrolyte layer. At high current densities, the formation of cracks was observed, with pillared deposits inside the cracks that led to electrical shortcircuits. At low current densities (lower 0.05 mA/cm^2) these phenomena were reduced significantly.
Many oxide electrolytes have a higher shear modulus than Sulphides. For example, the shear modulus of Al and Ta doped $Li_7La_3ZrO_{12}$ (LLZO) was calculated to be 56-61 GPa [42]. [27] conducted polarization tests with a current density of 0.5 mA/cm^2 for a Li-metal $Li_{6.75}La_3Zr_{1.75}Ta_{0.25}O_{12}$(LLZTO) cells with different relative pellet densities. With ex-situ SEM, they showed that Lithium can grow through grain boundaries and interconnected pores.
These findings suggest that Lithium metal plating with solid electrolytes depends on the current density, that bulk solid electrolyte may be strong enough to suppress dendritic growth, whereas connected pores and grain boundaries still allow it. The fact that cracks were observed in the pellet during fast cycling indicates strong local forces when Li-deposition happens in pores or along grain boundaries due to the large change in volume.

Although the mechanistic models of dendritic growth do not include SEI formation, it is generally accepted that the formation of a SEI has major effects on the morphology of the deposited lithium. Three ideal characteristics of the SEI have been proposed [16]:

- Uniform (fewer defects): A uniform SEI would promote uniform deposition of the Lithium metal, which reduces mechanical stress and thereby protects itself.
- Elastic: Elasticity of the SEI could help restraining the outward growth of Li-dendrites and could encourage mossy growth.
- Low (ionic) resistance: If the SEI is of low resistance, the diffusion of lithium ions is faster and therefore the probability of deposition at the substrate surface is higher. A phenomenon that can be illustrated by the Brownian statistical model.

1.1.3 Li_6PS_5Cl - Li-metal interface

There have been various studies about the interface between Li_6PS_5Cl and Li-metal, both computational and experimental. In this section, the ones known to the author are listed and the main findings relevant for this thesis are summarized.

[45] analyzed the stability of Li_6PS_5Cl with Li-metal using density functional theory. The phase equilibrium was found to be Li_3P, LiCl and Li_2S. A decomposition energy was defined as

$$E_D(\Phi) = E(phase\ equilibrium, \Phi) - E(solid\ electrolyte) - \Delta n_{Li}\mu_{Li}(\Phi) \tag{1.12}$$

where Δn_{Li} is the change in the number of Li-atoms from the solid electrolyte composition to the phase equilibrium. For this system, it was found to be -0.96 eV/atom, which indicates highly favorable reduction of the electrolyte. It is concluded that reported experimental stabilities are not because of thermodynamical stability, but due to sluggish kinetics of the decomposition reaction and the formation of a passivation layer with poor electronic conductivity similar to a SEI.

[6] performed molecular dynamics simulations with density functional theory to investigate the chemical processes at the Li-metal Li_6PS_5Cl interface at different temperatures.
The reaction was found to be:

$$(x + 5y + z - 6)Li + Li_6PS_5Cl \rightarrow Li_xP + 5Li_yS + Li_zCl \tag{1.13}$$

Where metallic Lithium is oxidized to Li+ supplying one electron, and P^{5+} is reduced to P^{3+} by breaking the P-S bond. The Li^+ was found to diffuse into the electrolyte, whereas the P^{3+}, S^{2-} and Cl^- diffuse to a lesser extent in the opposite direction into the electrode. The reaction started right at the beginning of the simulation, indicating a small energy barrier, and the decomposition increased with increasing temperature. It is noted that the reaction is most probably diffusion controlled. With simulated XRD the main decomposition products that were found are Li_2S, Li_3P and LiP. The formation of LiCl was indicated by a change in the Li-Cl radial distribution function.

[38] was able to experimentally identify the decomposition products LiCl and Li_2S using in-situ XPS. As third decomposition product they expected Li_3P, however, the binding energy of the compound is too close to the binding energy of the electrolyte. It was further found that the increase in resistance upon a few hours of contact was 20 Ohmcm^2, a factor two too high for an acceptable IR drop. The increase in resistance was modeled using the Wagner model for diffusion controlled solid-state reactions, assuming negligible electronic conductivity. Extrapolating the model to one year, SEI resistance of 300 Ohm cm^2 was found, and it was concluded that SEI formation may easily dominate the total impedance of a solid-state battery.

The electrochemical stability of the electrolyte vs. Li-metal was further investigated experimentally by [40] with CV measurements. It was found that when the voltage exceeded 2.2V vs Li/Li^+, the interface became electrochemically unstable, excluding the use of high potential positive electrode materials in combination with Lithium metal.

[44] prepared batteries with Li-metal and Li_6PS_5Cl and reported relatively good stability towards Li metal. They cycled a symmetric Li-Li cell at room temperature with a current density of 0.1 mA/cm2 over 4000 minutes and

66 cycles. This corresponds to a capacity of about 0.1 mAh per cycle. The apparent stability of the interface was attributed to a Li_2S buffer layer, that forms a protecting interphase.

Summarizing, Li-metal and Li_6PS_5Cl has been found to form an unstable interface by most sources and following decomposition products have been by DFT calculations proposed:

- Li_2S
- LiCl
- Li_3P
- LiP

The formation of Li_2S and LiCl have been confirmed experimentally by ex-situ XPS. Cells with Li-metal and the electrolyte have been shown to work and seemed (reasonably) stable in CV measurements up to 2.2 Volts versus Li/Li^+. Also regular cycling experiments showed apparent stability. It is proposed that this is due to a diffusion controlled interphase growth. The increase in resistance because of the interphase growth was found to be larger than acceptable. No studies are currently known to the author where specifically dendrite growth was investigated for this system.

1.2 Theoretical background of measurement techniques

1.2.1 Neutron depth profiling

Neutron depth profiling can be used to nondestructively measure Li-concentration profiles in materials with up to 40um depth. When the electrode/electrolyte interface can be placed within those 40 microns, the Li-ion concentration profile at the interface can be measured. In this section, the measurement mechanism is explained, the experimental setup is described and the data analysis is introduced. The sections "Mechanism of the measurement" and "Measurement setup" are based on the manual Neutron depth profiling basics written by Tomas Verhallen.

Mechanism of the measurement

In neutron depth profiling, a thermal neutron is captured by the nucleus of an element which decays exoergically. Depending on the specific reaction, a particles with a well-defined energy are emitted. Due to the low momentum of the incoming neutron, the reaction center can be attributed to the initial location of the atom. The reaction of ^{6}Li is shown in Equation 1.14.

$$^6Li + n \rightarrow ^4 He(2055keV) + ^3 H(2727keV) \tag{1.14}$$

The amount of reactions that happen within a time frame is proportional to the concentration of active isotopes, the Neutron flux, and the neutron capture cross section. The emitted ions, in this case the Triton and the alpha particle, are emitted in all directions. During their path through the surrounding matter, the ions loose energy through collisions with the surrounding matter. At the detector, the residual energy of the ion is measured. With knowledge about the stopping power of the surrounding matter, the depth of the reaction center can be calculated.

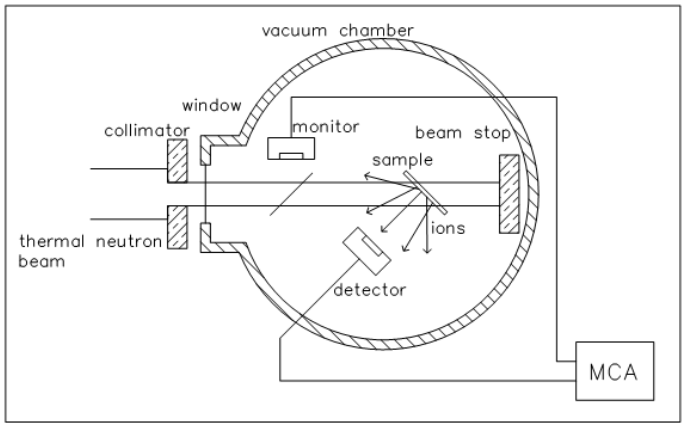

Figure 1.3: Schematic setup for a neutron depth profiling experiment. Figure form Tomas Verhallen's Neutron depth profiling basics.

Measurement setup

A typical setup for a NDP measurement is shown in Figure 1.3. The neutron beam enters the chamber through a collimator and hits the sample at an angle. Due to the low interaction of neutrons with matter, it can be assumed that the beam intensity is homogeneous within the sample. If significantly ^{6}Li enriched samples are measured, or casings with high scattering cross sections are used, this would have to be investigated further. The detector is then placed in plane with the sample surface. The detector measures the signal of the ionized particles and high energy gamma radiation, which can also come from the activation of components inside the setup. Therefore, the measurement has to be background-corrected. The detector used is a Multi channel analyzer (MCA) which operates in pulse height analysis mode. The detector efficiency for different channels is calculated by measuring a known boron standard. A second detector measures the signal of a thin piece of foil with ^{6}Li on it. The count rate from this detector is used to monitor the neutron flux and for dead time correction of the MCA.
As the residual energy of the particle depends on the path length of the tritons, the geometry of the setup plays an important part in the resolution of the measurement. When d is the distance between the sample plane and the detector surface, then the path length x of a particle is

$$x = \frac{d}{cos(\alpha)} \tag{1.15}$$

It is clear that when α is 90 degrees, then the path length is smallest and equals d. Assuming that the center of the sample and the detector are perfectly aligned, the maximum path length be calculated easily using Pythagoras. The maximum difference in path lengths can therewith be written as

$$\Delta x = x_{max} - x_{min} = \sqrt{d^2 + (r_{sample} + r_{detector})^2} - d \tag{1.16}$$

From the equation it is clear, that Δx is small when d is large compared to r_{sample}+$r_{detector}$. Therefore, the detector is placed relatively far away from the sample. To minimize the energy loss during the path through air, the system is kept at lowered pressure.

Data analysis

There are several ways to analyze NDP spectra. Here a summary based on the review in [32] is given.

The simplest and most common way to analyze an NDP-spectra is to calculate the depth corresponding to a specific channel in the MCA using the stopping power of the material. This relation can be expressed as

$$N(E) = N(x)\left(-\frac{dx}{dE}\right) = c(x) f_{ion} \overline{\sigma}_{ion} \Phi_t \left(\frac{\epsilon A_n}{cos(\Theta_n)} \frac{A_d}{4\pi r_d^2} \frac{cos(\Theta_s)}{S(E)}\right) = \kappa \frac{C(x(E))}{S(E)} \tag{1.17}$$

where N(E) is the amount of counts at energy E, *c(x)* the concentration profile of the ion, f_{ion} a correction factor for the isotope concentration, $\overline{\sigma}_{ion}$ thermal the averaged cross section, Φ_t the thermal neutron flux, ϵ the detector efficiency, $\frac{A_n}{cos(\Theta_n)}$ the sample surface illuminated by the neutron beam, $\frac{A_d}{4\pi r_d^2}$ the probability of a generated ion reaching the detector, Θ_s the angle of the ion path to the sample normal, and S(E) the stopping power of the material. The concentration profile can then be obtained by

$$C(x) = \frac{1}{\kappa} N(E(s)) S(E(s)) \tag{1.18}$$

if N(E) is known. N(E), however, has to be estimated from the MCA channel counts y_i. The number of counts in a channel *i* for a measurement time Δt are

$$y_i = \Delta t \int_{E_t+\Delta}^{E_t-\Delta} N(E) dE = \frac{\kappa \Delta t}{cos(\Theta_d)} \int_{x(E_t-\Delta)}^{x(E_t+\Delta)} C(x) dx \tag{1.19}$$

where the concentration profile was substituted into the equation for N(E). This leads to a form

$$y_i = \int_0^{x_{max}} c(x) R_i(x) dx \tag{1.20}$$

where $R_i(x)$ is the channel response function given by

$$R_i(x) = \begin{cases} \frac{\kappa \Delta t}{cos(\Theta_d)} & \text{if} x(E_i + \Delta) < x < x(E_i - \Delta) \\ 0 & \text{otherwise} \end{cases}$$

If N(E) varies only slightly over a channel width, equation 1.19 can be approximated by $2\Delta N(E_i)\Delta t$, so that $N(E_i) \approx \frac{y_i}{2\Delta \Delta t}$, such that

$$C(x_i) = C(x(E_i)) = \frac{y_i}{\Delta T} \frac{S(E_i)}{2\Delta \kappa} \tag{1.21}$$

However, this simple approach neglects several aspects that influence the amount of counts measured at a certain energy:

- Energy straggling: The energy loss by collisions is a stochastic process which leads to slightly different energies for particles that traveled the same distance. Additionally, small angle scattering inside the material leads to different path lengths. These two phenomena together will be referred to as Energy straggling. Energy straggling can be investigated using TRIM (Transmission and Range of Ions in Matter) simulations and can be described by a Gaussian model.
- Detector energy-broadening, which results from electronic noise in the amplifier chain, intrinsic noise caused primarily by leakage currents and because in addition to ionizing interactions, some energy is lost to phonon production. Detector energy broadening can also be described by a Gaussian model.

- Geometric broadening: Difference in path length due to the finite size of sample and detector. Geometric broadening is non-Gaussian, but the contribution can often be neglected compared to the other effects if the setup geometry is chosen well.
- The amount of counts inside a channel follow Poisson statistics and therefore has an error of $\sqrt{N}$.

The system with Gaussian energy broadening can be expressed as in equation 1.20, but with the response function (neglecting geometrical broadening)

$$R_i(x) \approx \frac{\hat{\kappa}}{2}\left[erf\left(\frac{E_i + \Delta - \overline{E}(x/\omega_s)}{\sqrt{2}\sigma(x/\omega_s)}\right) - erf\left(\frac{E_i - \Delta - \overline{E}(x/\omega_s)}{\sqrt{2}\sigma(x/\omega_s)}\right)\right] \tag{1.22}$$

To obtain the concentration profile c(x), Equation 1.19 has to be solved for each channel *i* and response function $R_i(x)$. The total standard deviation arising from the individual contributions can be calculated as follows

$$\sigma = \sqrt{\sum_{i=1}^{N} \sigma_i^2 s} \tag{1.23}$$

This kind of unfolding problem is known as the Fredholm integral equation and is often approximated by

$$y_i = \sum_{j=1}^{M} R_{ij} u_j,\ i = 1, ..., N \tag{1.24}$$

where $u_j = C(x_j)$ and R_{ij} depends on the quadrature approximation used. Often, equation 1.24 has no unique solution as the amount of unknowns M is most likely different from the number N of measured data. Several approaches to circumvent this problem have been developed. Probably the most intuitive approach is to make an assumption about the shape of the concentration profile where the free parameters are estimated by minimizing χ^2. However, other iterative methods and Fourier transform methods have also been proposed. Each of these different methods have their own advantages and disadvantages and their applicability depends on the system measured and on the results that one wants to extract from the measurement.

Stopping Power

The stopping power is an atom specific function that describes the energy loss of an ion at a specific energy when traveling through a unit distance in space. The stopping power of a elemental material is described by the Bethe-Bloch equation

$$S = \frac{dE}{dx}s = \frac{\kappa Z_2}{\beta^2} Z_1^2 L(\beta)\ \left[\frac{keV}{um}\right] \tag{1.25}$$

where $\kappa = 4\pi r_0^2 m_e c^2$, L is called the stopping number, Z_1 is the atomic number of the Nuclei of the ion, Z_2 of the target material, and β the relative particle velocity v/c. The stopping power of compounds can be calculated using the stopping power and range of ions in matter (SRIM) calculator or the simulation package Transmission and Range of ions through matter (TRIM) [46].
SRIM makes an approximation known as Bragg's law, which states that the stopping power of a compound is the same as the sum of the stopping power of the individual elements. This can be easily derived by assuming that the material consists of very thin sheets of elemental matter. This approximation assumes that the electron density is homogeneous across the compound. For materials with complex bondings and therefore large deviations in electron density, this is not valid. Therefore, a compound correction can be included. For Li_6PS_5Cl, it would

probably be necessary to investigate whether the P-S bonds leads to such a deviation. However, no previous study about such compounds was found in the literature study preceding this research project. For SRIM 2010 the accuracy of the Stopping power calculations was determined by comparison with experimental data. For H-ions, 87% of the experimental data was found to be within 10% of the SRIM calculation, and 74% within 5% [47].
TRIM is a Monte Carlo Computer program which calculates the interaction of a chosen ion with a target, which can consist of different layers which are assumed to be amorphous [3]. When simulating the energy of transmitted ions for different depths of the battery, a similar energy versus depth relation can be obtained. TRIM gives somewhat more information than SRIM, as the energy distribution of the particles after transmission through the material is known, including deviations caused by ions with different path lengths.

Neutron Depth profiling on solid-state batteries

Few papers have been published about Neutron depth profiling spectra of electrodes and of liquid electrolyte batteries. Only two papers are known to the author, where NDP was applied to all-solid-state batteries.

[25] did in-situ studies of Li-ion all-solid-state micro batteries. By preparing the $LiCoO_2$ with 100% ^{6}Li, and leaving the electrolyte (LiPON) at the natural abundance level of 7.5%, it was shown that, prior to cycling, no Lithium exchange happens between the Cathode and the Electrolyte. Upon starting, the ^{6}Li concentration decreased quickly at the edge of the electrode. This was explained by two phenomena: the formation of a concentration gradient inside the electrode while charging, and an increased exchange of ^{6}Li and ^{7}Li at the interface. It was also shown that the ^{6}Li concentration gradient in the electrolyte equilibrated after 2 hours, while the profile in the cathode stayed the same, indicating a much higher Li-ion mobility in the electrolyte.

[36] did in-situ neutron depth profiling of Li-metal plating with a Garnet electrolyte. They assembled two cells, one symmetric lithium cell and one Li-metal Carbon nanotube cell (CNT). Cross sectional SEM images showed good contact for the Li-metal Garnet interface, and poor point contact between the Garnet and the CNT. The interface between the Garnet and the CNT did not cycle reversibly, and an accumulation of Lithium in the CNT was observed with NDP. Both the cycling performance as well as the NDP counts showed reversible behavior in the symmetric cell. Shortly before a short-circuit formed, the NDP counts increased in several energy ranges next to the window. The accumulation is explained by a normal plating regime when plating on the window, but a partial short-circuit during stripping, which was named a "dynamical short-circuit".

1.2.2 Powder diffraction

Powder diffraction can be used to determine the crystal structure of a sample. A crystal structure is generally defined by a unit cell which is repeated periodically in a specific lattice. When a incident wave meets a atom inside the lattice, the wave is reflected. If the wavelength is the same size or shorter than the inter atomic distances, interference patterns will form from the waves incident on atoms in planes parallel to each other. Constructive interference can be found where the Bragg condition is fulfilled:

$$n\lambda = 2d_{hkl}sin(\Theta) \tag{1.26}$$

Where λ is the wavelength, d_{hkl} the distance between the planes, and Θ the incident angle of the beam to the

plane. In a powder sample, there are many small crystal grains which are oriented in different ways. A beam incident on a powder sample therefore creates interference maximas at angles corresponding to all planes that can be found in a crystal.

Peak broadening of the diffraction data can give information about the crystallite size, which is described by the Debye-Scherrer Formula:

$$p = \frac{18000 * K * \lambda}{\pi X} \tag{1.27}$$

where p is the particle size in Angstrom, K the Scherrer constant (typically around 1), λ the wavelength and X the full with at half maxima of the diffraction peak [15]. Diffraction experiments can be made with both x-rays and neutrons. X-rays have advantages in signal intensity, price and availability. Due to the interaction with electrons, x-rays are more suitable for materials containing heavy atoms. Neutrons have the advantages that they are non-destructive and that even some light atoms, like Lithium, have large scattering cross section. Accurate Information about the site occupancy of Li-atoms or about the thermal parameters are better extracted from neutron diffraction measurements.
To analyze the intensity vs. angle data, a technique known as Rietfield refinement is used. In a Rietfield refinement, a model of the crystal is made and different parameters are estimated using a least square fit.

1.2.3 Solid state Nuclear Magnetic Resonance

NMR can be used to investigate the local chemical environment or dynamics of isotopes with a spin. Compared to x-ray diffraction, it is also sensitive to amorphous materials, which makes it a useful complementary method for material characterization. NMR is unique when it comes to measuring chemical exchanges and diffusion properties of materials. However, a description of how solid-state nuclear magnetic resonance (NMR) works is outside the scope of this thesis. In this section, the basic theory for one-pulse NMR measurements is briefly outlined. The information given can be found in various textbooks and is therefore considered general knowledge. Some practical considerations are listed. An extensive review about the use of NMR in the research field of batteries can be found in [26].

Basic theory

When an isotope with a spin is placed in a magnetic field B_0, the energy levels of the different spin states split up, which is known as the Zeeman effect. The isotopes align themselves according to their energy level. The spin $1/2$ (parallel to B_0) or -$1/2$ (anti parallel to B_0) form two populations whose equilibrium ratio is Boltzmann distributed

$$\frac{N_-}{N_+} = exp\left(-\frac{\Delta E}{kT}\right) \tag{1.28}$$

An isotope can be excited under absorption of a photon under absorption of a photon with frequency

$$\omega = \gamma(1-\sigma)B_0 \tag{1.29}$$

where γ is the gyromagnetic ratio, σ the chemical shift tensor and B_0 the applied magnetic field. ω is generally called the resonance or the Larmor frequency. The Zeeman interaction is the same for all nuclei of a given type.

However, the electron density around the nuclei lead to shielding/deshielding of the effective field from the nuclei expressed as σ, which modifies the precession frequency [31].

The magnetic field of the spin packets can be represented by a net magnetization vector, which consists of the sum of all individual magnetic moments. In equilibrium, the net magnetization M_0 is aligned with the external magnetic field B_0, which is conventionally aligned with the z-axis. When an external pulse with resonance frequency is applied, the net magnetization will shift from its equilibrium state into the XY-plane. The angle of the net magnetization to B_1 depends on the pulse length τ and the magnitude of the field B_1.

$$\theta = 2\pi\gamma\tau B_1 \tag{1.30}$$

After the pulse, the excited system will decay according to the equation

$$M_z = M_0 \left(1 - exp\left(\frac{-t}{T_1}\right)\right) \tag{1.31}$$

Where T_1 is the spin lattice relaxation time.
The magnetization in the XY plane will rotate around the z-axis at a frequency equal to the Larmor frequency. Initially, the individual components all point in the same direction. However, due to small differences in the local magnetic field, spin packages have a slightly different Larmor frequency, which leads to an increasing phase shift also called spin-spin relaxation. The reason for the different Larmor frequency can be molecular interactions (pure T2 molecular effect) or inhomogeneities of B_0 (inhomogeneous effect).

$$M_{XY} = M_{XY0} \left(1 - exp\left(\frac{-t}{T_2}\right)\right) \tag{1.32}$$

The relationship between the (change in) magnetization, T_1 and T_2 are described by the Bloch equations:

$$\frac{dM_{x'}}{dt} = (\omega_0 - \omega)M_{y'} - \frac{-M_{x'}}{T_2} \tag{1.33}$$

$$\frac{dM_{y'}}{dt} = -(\omega_0 - \omega)M_{x'} + 2\pi\gamma B_1 M_z - \frac{M_{y'}}{T_2}s \tag{1.34}$$

$$\frac{dM_z}{dt} = -2\pi\gamma B_1 M_{y'} - \frac{M_z - M_{z0}}{T_1} \tag{1.35}$$

The rotating magnetic fields in the XY-plane induce a voltage in a coil wire that is placed around the sample. The voltage is measured, the FID, which is an overlay of the signal generated by all the different frequency components. By Fourier transforming the FID, the different frequency components of the signal can be identified. Integrating the area under the curve (if the signal is well phased) gives the ratio of atoms in a specific chemical environment. As the Larmor frequency is dependent on the applied B_0, the chemical shift

$$\delta = \frac{\nu_{sample} - \nu_{ref}}{\nu_{ref}} \tag{1.36}$$

was defined as a more general measure. ν_{sample} is the Larmor frequency of the sample that is measured. ν_{ref} is the frequency of the reference compound measured at the same magnetic field strength. The reference compounds are specified standards for each element.

Onepulse experiments and some experimental considerations

The simplest NMR experiment is a so called one-pulse experiment. In it, the net magnetization of the sample is excited to a specific angle (in solid-state NMR often 90 degrees), and the voltage decay is measured (the FID) and Fourier transformed. From there, information about the chemical shift and the relative amount of chemical environments of the measured isotope can be derived. The Larmor frequency can be related to a specific compound which is called fingerprinting.

To get a good signal, there are two primary aspects of importance: the signal to noise ratio and the line width. The signal to noise ratio depends on the signal intensity and the amount of scans that are taken. The signal intensity measured with NMR depends on the difference between the populations of the different spin states. This difference increases with the energy difference between the spin states (Equation 1.28). The energy difference is also proportional to the Larmor frequency (Equation 1.29) and the signal intensity is therefore proportional to B_0 and the gyromagnetic ratio of the nuclei. This is the reason why, in practice, very large B_0 fields are needed. Nuclei with high gyromagnetic ratios can also lead to a greater signal magnitude, however the natural abundance of the nuclei also needs to be considered. The difference in sensitivity of a nuclei can be calculated.

$$n = \frac{\gamma_a^3}{\gamma_b^3} \frac{abundance_a}{abundance_b} \tag{1.37}$$

where nuclei *a* is *n* times more sensitive than nuclei *b*. High signal intensity is important as the final spectra should have a good signal-to-noise ratio. When the signal intensity is high, fewer scans are needed to measure the same spectra, which can have large influence on the measurement time and therefore also on the cost.
Another important property for good measurements is the line width, as it is an indication of how well resolved the spectra is. The line width is influenced by several factors:

- Relaxation time
- Instrumental aspects
- Signal acquisition
- Sample problems
- post processing

The relaxation time is a function of many fundamental properties of the material. A thorough discussion of the relaxation time is out of the scope of this thesis. As a rule of thumb, relaxation is mainly determined by T_2; low T_2 leads to a broad line width. In liquid NMR, the tumbling/rotating of the molecules inside the liquid leads to large relaxation times due to motional averaging of anisotropic interactions. In a solid, this is not the case. To get narrower line widths in solid, artificial motional averaging is achieved by a technique called Magic Angle Spinning (MAS), where the sample is spun at an angle of 54.74 degrees. Spinning frequencies reach up to several tens of thousands of Hertz.
There are many instrumental factors that can lead to line broadening. Examples are inhomogeneities in B_0 or poor tuning. Sample problems can be caused by inhomogeneous samples arising from bad mixing, temperature gradients across the sample or paramagnetic impurities.
There are two characteristic phenomena that result from bad signal acquisition, Clipping and Truncation. Clipping is a phenomena that happens when the receiver gain is too high and part of the signal is cut off at the

beginning of the spectra. Fourier transforming such a spectra broader line widths are observed. Truncation happens when the Acquisition time is too short and the last part of the FID is cut off. When Fourier transforming such a signal, this leads to ripples around the peak. Post processing techniques can be used to improve the line width, however it always comes at the cost of sensitivity.

2. Material and Methods

2.1 Research objective

The main focus of this thesis is to develop a cell setup for NDP measurements with a solid-state electrolyte and Li-metal as Anode. Therefore, the requirements of the cell are defined, an initial design is proposed, implemented, and the electrochemical performance of the cell is tested under different circumstances.
For comparison with the NDP-cell, preliminary electrochemical measurements for Li-metal cells with the electrolyte Li_6PS_5Cl are conducted in regular solid-state cells and the electrochemical performance is assessed.
The stability of the interface between the materials is investigated with ex-situ XRD and ex-situ solid-state NMR measurements. To do so, also the pristine electrolyte was characterized thoroughly.
Finally, standard NDP data analysis was implemented, and the depth uncertainty due to Energy straggling was investigated, and initial NDP measurements were performed to test the cell, and further design improvements are suggested.

2.2 Experimental details

Synthesis Li_6PS_5Cl

To synthesize the electrolyte, the precursor Li_2S, P_2S_5 and LiCl are weighed according to their stoichiometric ratio. In this thesis, always 1378.4 mg Li_2S, 1333.65 mg of P_2S_5 and 508.75 mg LiCl were mixed with 5 Tungsten Carbide ball mills (8g each) with 110 RPM for 20 cycles of 3 minutes with 1 minute rest in between. The powder mixture is poured into silicon glass vials and sealed under argon atmosphere. The sealed sample is heated at 550 degrees Celsius for 10 hours with a heating and cooling rate of 100 degrees per hour. The glass vial is opened in an argon-filled glove box, and grounded to a powder by hand. Every single batch is tested with XRD to control whether the material is pure-phase.

Solid state cell assembly

Due to the reactivity of the Argyrodite and the Li-metal, all cells were prepared in an Argon filled glovebox with around 0.1 ppm Oxygen and 0.9 ppm H_2O. The electrolyte pellet was first pressed with 5 MPa. The Lithium or Indium foils were then put on the pellet surface and pressed with 0.5 Mpa. For cells used for ex-situ measurements, stainless steel foils were put between the Lithium/Indium foil sheets and the associated current collector to avoid the metals to stick to the current collector.
From experience, many batteries suffered from internal short cuts when:

- The electrolyte pellet was too thin
- The Lithium metal foil was too thick
- The Lithium metal was pressed on with higher pressure

Therefore, the Lithium foil was rolled thinner between two clean plastic foils. This had the additional advantage of reducing surface impurities. O-rings and proper component placement was critical to ensure that the cells were airtight.

Electrochemical measurements

All cells were cycled galvanostatically on a Maccor 400A regulated for rated currents of 5A, 150mA, 5mA or 150uA. The Lithium vs. Indium cells and the symmetric Lithium cells were all cycled up to a maximum capacity of 0.2mAh. The Lithium vs. Titanium cells were also cycled up to 0.2 mAh, but had an additional voltage cutoff criteria due to irreversible cycling.

XRD

X-ray diffraction on an X'Pert Pro X-ray diffractometer (PANalytical) using a copper target ($1.5406*10^{-10}$ m at 45 kV and 40 mA) in the 2Θ range from 0 to 90 degrees. The Rietfield refinements were performed with GSAS [15] and the graphical user interface EXPGUI [34]. As a starting point for the refinements neutron diffraction data was used (See Annex Table 6.2-6.1, thanks to Jart Hageman for supplying it).

NDP

The electrolyte pellet for the NDP cell was pressed in an external pellet press with 10 MPa and then inserted into the assembly. The pellet density was calculated from the pellet weight and volume (Table 2.1). The density was used as input for SRIM and TRIM to calculate the stopping power.

Table 2.1: NDP electrolyte pellet

Weight	0.15	gram
Height	0.12	cm
Area	0.79	cm^2
Volume	0.09	cm^3
Density	1.59	g/cm^3

As for the regular cells, the Lithium metal was rolled out and pressed with 0.5 MPa.
Due to the exploratory nature of the measurements and limited beam time, no standard methodology was used for the measurements. For the background measurement, the cell was assembled completely with window and electrolyte but without plated Lithium. The difference between the actual measurement and the background measurement therefore only shows additional lithium metal due to plating or doping with ^{6}Li.

NMR

Solid-state NMR measurements were performed on a Bruker Ascend 500 spectrometer (B_0 = 11.7 T) equipped with a NEO console, the operating parameters set as documented in table 2.2. For the measurements of the electrolyte, the parameters of the pristine electrolyte are documented. The deviations for the cycled electrolyte are minor. For the measurements of the electrolyte and Li_3P, T1 was determined and the recycle delay was set to 3 times T1. For Li_2S, T1 has not been determined because it turned out to be extremely long. For LiCl T1 was also not determined. Thanks to Yaolin Xu for supplying the measurements for Li_3P and to Violetta Arszelewska for the measurements for Li_2S.

Table 2.2: NMR measurement parameters

Measurement	Spectrometer frequency	Offset	Pulse-power	$\pi/2$ pulse-length	Reference	MAS
^{7}Li Electrolyte	194.38 MHz	321.40 ppm	60W	4.8 us	LiCl	12kHz
^{6}Li Electrolyte	73.60 MHz	170.96 ppm	300W	4.5 us	LiCl	12kHz
^{31}P Electrolyte	202.47 MHz	268.25 ppm	96W	3.7 us	H_3PO_4	12 kHz
^{6}Li Li_3P	73.60 MHz	339.65 ppm	300 W	4.5 us	LiCl	24 kHz
^{31}P Li_3P	202.47 MHz	961.13 ppm	65 W	4 us	H_3PO_4	24 kHz
^{6}Li Li_2S	73.60 MHz	339.65 ppm	300W	4.5 us	LiCl	20 kHz
^{6}Li LiCl	73.60 MHz	358.65 ppm	300W	4.5 us	LiCl	12 kHz

3. Results

3.1 Electrolyte characterization

The pristine electrolyte was characterized with XRD, TEM with EDX and solid-state NMR.
In Figure 3.1 (left) a diffraction pattern of Li_6PS_5Cl is shown. The refinement has an wRp of 0.0607 and Rp of 0.0437, no major impurities were detected. The background covers 85% of the area. Part of the background at low angles may arise from the Kapton covered sample holder, but part of the electrolyte is most probably amorphous. When calculating the crystallite size from the peak broadening, a size of 92.5 nm is obtained.
In Figure 3.1 (right), two diffraction patterns of the same electrolyte batch are shown. The data was normalized to an area of one for comparison, hence the low intensity. The peaks are shifted in 2Θ, which probably arises from instrumental aspects. For I_2, the peaks at 25.5 and 52.5 degrees are of higher intensity compared to I_1. The reflections belong to the (220) and (440) planes of the crystal. The reflections at 15, 30 and 31.5 degrees are lower for I_2. These reflections belong to the (111), (311) and (222) planes. As the electrolyte is from the same batch, it can be assumed that the structure is the same and that the differences arise from the sample preparation or the holder.

In Figure 3.2, the ^{6}Li and ^{31}P solid-state NMR spectra are shown. For ^{31}P, one broad peak was detected at 84.1

Figure 3.1: Left: XRD pattern of pristine Li_6PS_5Cl. Right: Two XRD pattern of the same electrolyte.

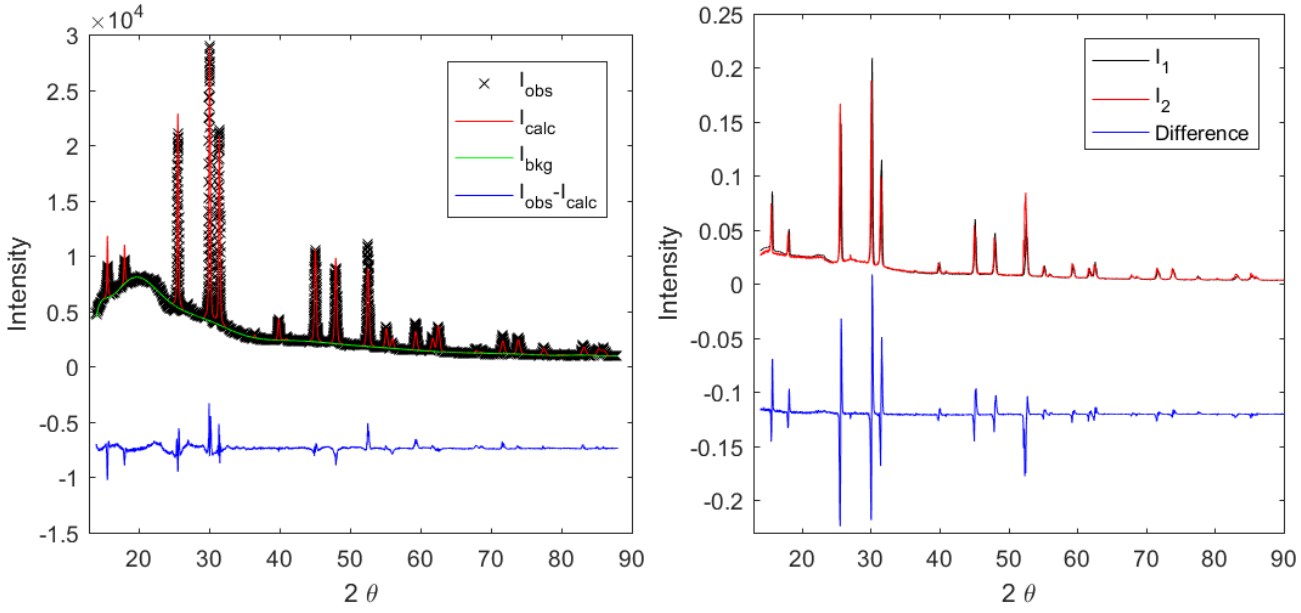

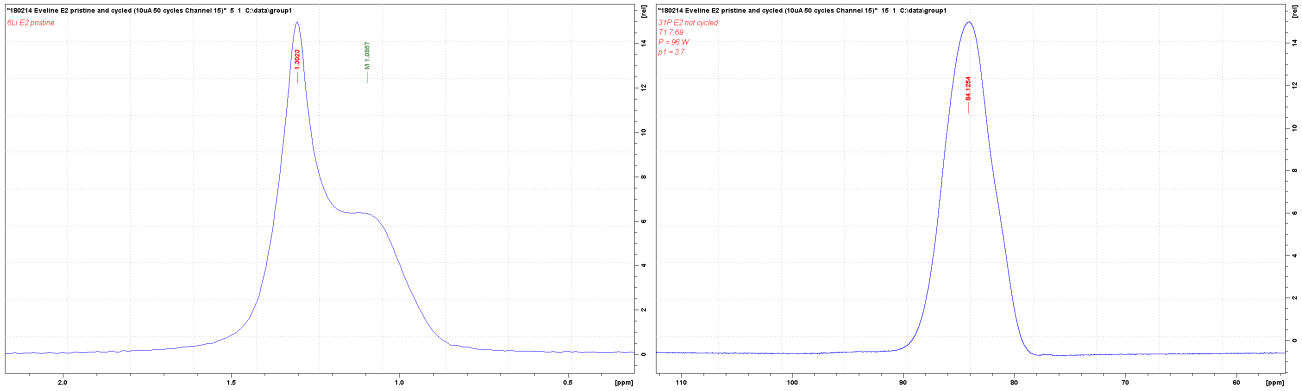

Figure 3.2: ^{6}Li (left) and ^{31}P (right) NMR spectra of pristine Li_6PS_5Cl. ^{7}Li can be found in Figure 6.2 in the Annex.

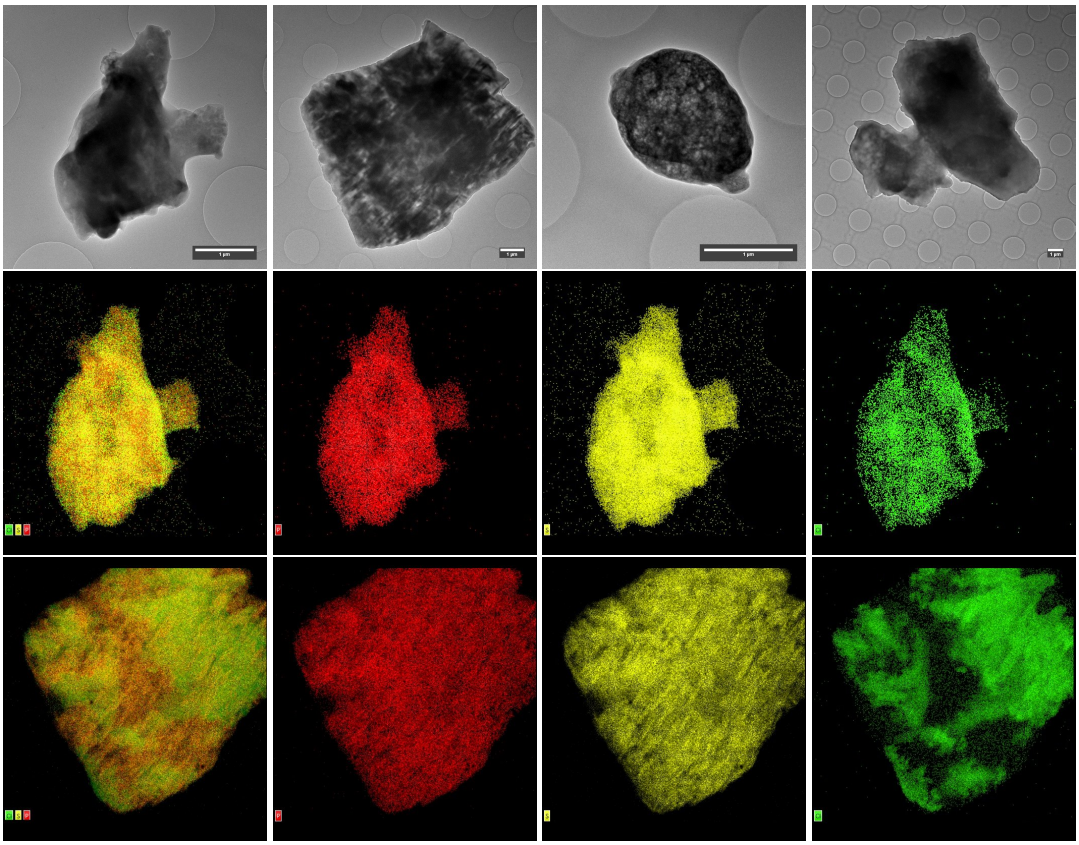

Figure 3.3: Top row: TEM images of four different Li_6PS_5Cl particles. Middle row: EDX spectra of the first particle. Bottom row: EDX spectra of the second particle. Sulfur atoms are represented in yellow, Phosphorous in red, and Chlorine in green. Thanks to Shibabrata Basak.

ppm. In literature, three overlapping peaks were reported at 85.1, 83.6 and 81.6 ppm [9]. The measurements were conducted at slightly higher spinning speed (15kHz), therefore the spectra may be better resolved. For Lithium, two peaks were detected at -1.3 and -1.1 ppm.

In Figure 3.3, TEM images of four particles (first row) and EDX spectra corresponding to the first two particles are shown. The images indicate that the particle size range is quite large, with sizes from 1.65 um diameter (particle 3) to more than 10 um (particle 4). The particles also have different shapes. This, and because the crystallite

size from XRD was much smaller, can raise the assumption that the crystallites agglomerate. The EDX spectra showed uniform elemental distributions across the first particle, the second particle only shows uniform P and S distribution, while there are regions that are depleted of Cl. Considering the uniform P and S distribution it is unlikely that shading effects are the cause.

3.2 Electrochemical performance of the batteries

To test the electrochemical performance, Li-metal vs. indium and symmetric Li-metal cells were cycled galvanostatically, at a maximum capacity setting of 0.2 mAh and at different current densities (Figure 3.4). The batteries cycled with 100% capacity retention. The voltage spikes for the batteries cycled at 10 and 20 uA are there because the conductive case of the battery touched the case of another cell.
Between 10 and 30 uA, the battery cycled stable with a small and steady increase of the overpotential. At 40uA, the battery cycled stable except for the period between cycle 20 and 30, where the voltage plateau is distorted during charging the battery, with a voltage lower than the usual charge voltage, which resembles the "dynamic short-circuit condition" reported in [36]. However, the battery returns to normal operation after for 20 more cycles. The same accounts for the battery at 50uA between cycle 6 and 38 (see Annex Figure 6.1). The overpotential is generally very low and increases with the amount of cycles. The overpotential also increases when cycling at 10uA, 20uA and 30uA, but then drops when the current is increased to 40-50 uA. At 60 and 70uA, the overpotential again increased, but not to values as at 30uA.

Figure 3.4: Electrochemical performance of Li-In cells cycled galvanostatically at different current densities and maximum capacity of 0.2mAh.

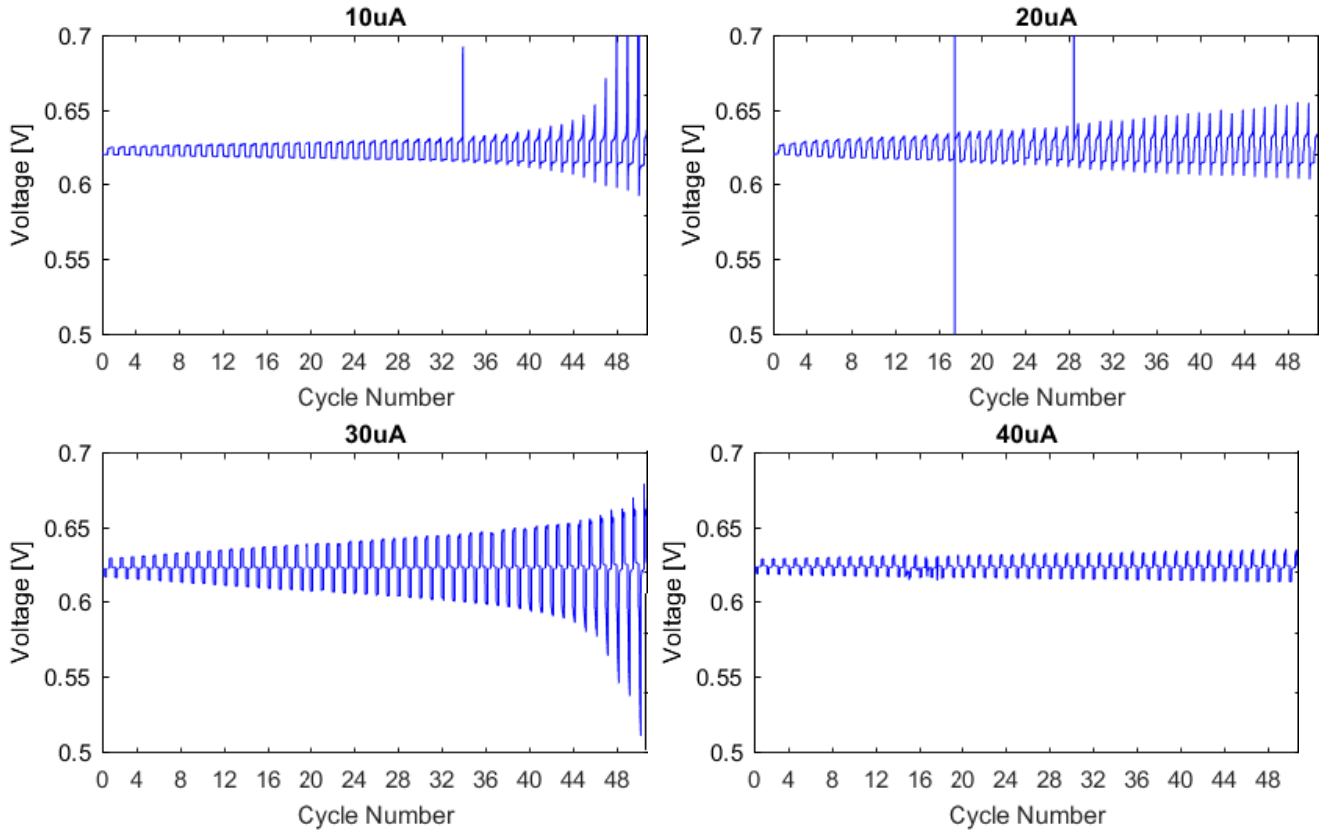

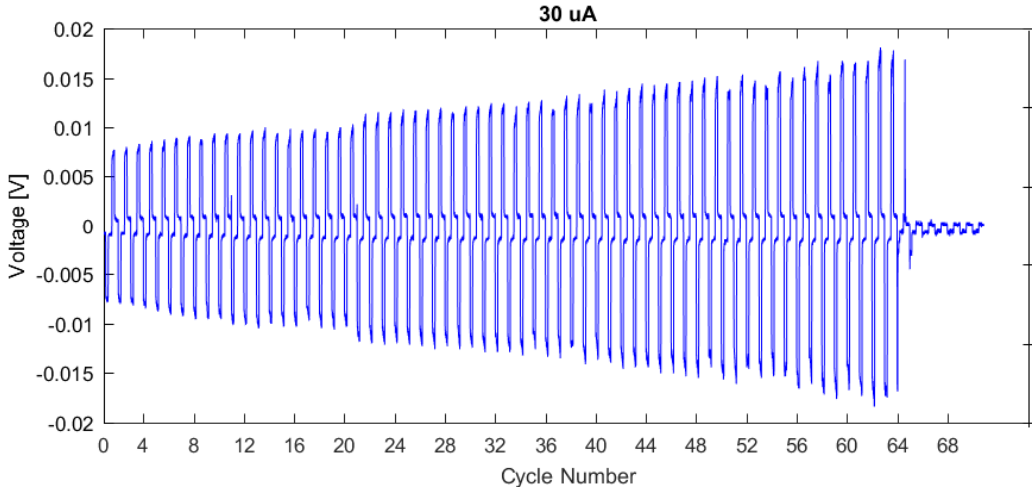

Figure 3.5: Electrochemical performance Li-Li symmetric cell cycled at 30uA and 0.2mAh

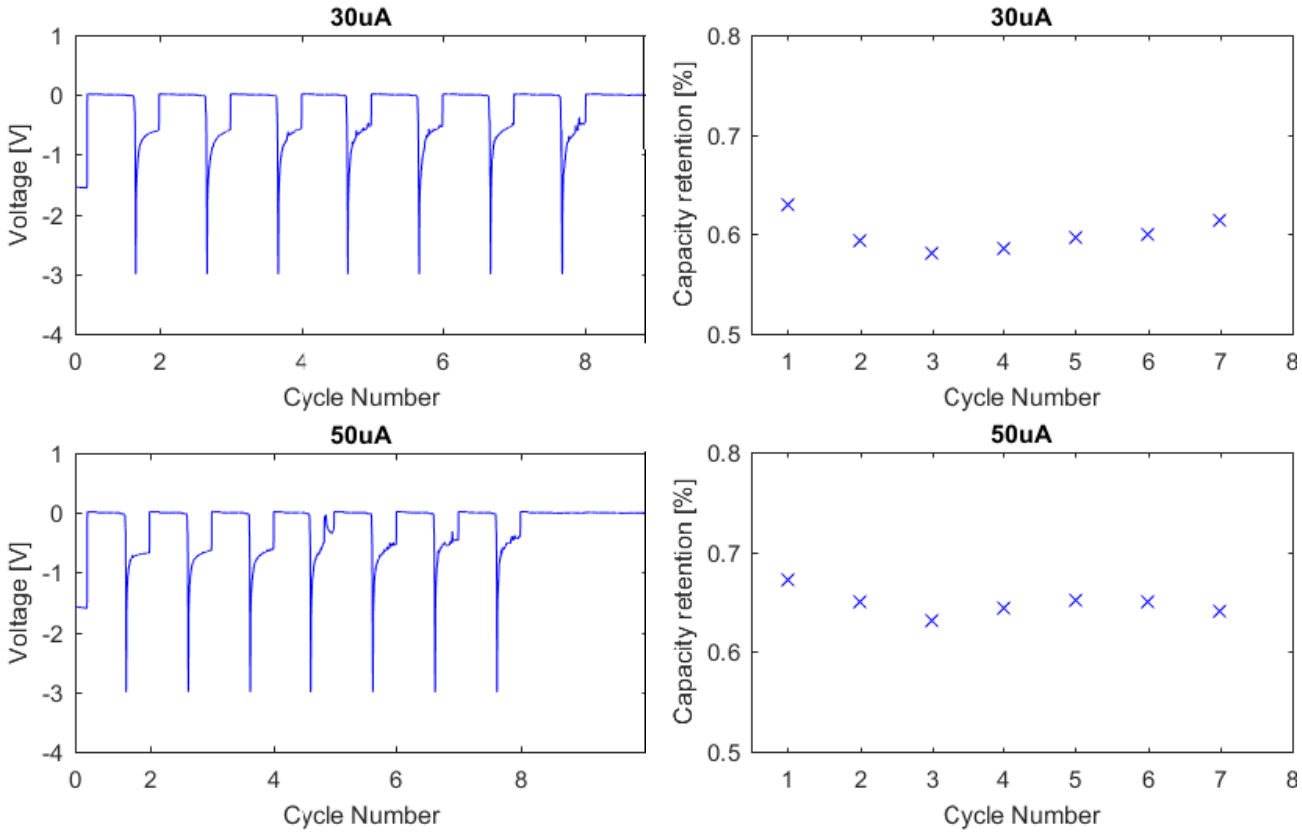

Figure 3.6: Electrochemical performance of Li-titanium cells

In Figure 3.5, an example of a symmetrical Li-Li cell is shown. The cell cycled well for 64 cycles, with a continuous but small increase in overpotential, until it short-circuited.

As preparation for the NDP cell, Lithium metal was also plated on titanium foil (Figure 3.6).The open circuit potential was non-zero due to the different potential of the titanium surface. During the first plating, the voltage quickly went to the regular Li-plating voltage after the first nucleation. Then, compared to the Lithium-Indium

system, not the whole capacity could be retained. Therefore, a cutoff voltage of three volts was selected. Around 40% of the Lithium was lost for each cycle with these settings. There are several other reasons why the capacity retention in the lithium-titanium cells could be so low:

- There is a decrease in volume upon stripping, as the materials are not elastic this can lead to loss of contact of the lithium metal to the argyrodite. This could also be the cause for the formation of the rings described above.
- The Lithium can grow into the electrolyte, and the stripping process may lead to an interruption of the electrically conductive path and therewith electrically insulated/ dead lithium chunks.
- The formation of decomposition products between the Argyrodite and the Lithium metal.

Finally, the cells short-circuited a lot more quickly compared to the Li-Li and the Li-In cells.

3.3 Ex-situ measurements

3.3.1 Ex-situ XRD

To investigate changes of the crystal structure of the electrolyte or the formation of new crystalline phases, ex-situ XRD measurements were conducted (Figure 3.7). Therefore, the battery was disassembled, the electrolyte scraped off from the electrodes, ground by hand in a mortar and put in the Kapton covered XRD holder. The electrolyte was obtained from a Li-Indium cell after 100 cycles of 0.2 mAh at 30uA. Only the Li_6PS_5Cl phase was refined. Except additional peaks at around 33 degrees no major changes can be detected compared to the pristine electrolyte. Compounds with Bragg reflections in the area are LiOH, Li_3PO_4 , Li_2S and Li_3P. The measurement was conducted four times for one hour, and it could be observed that the peaks grew during subsequent measurements (not shown). It is therefore most plausible that the electrolyte reacted with H_2O or O_2, partially maybe while cycling the battery, and partly because the sample holder leaks, or because of water trapped in the sample holder (which was dried in a heated vacuum oven).

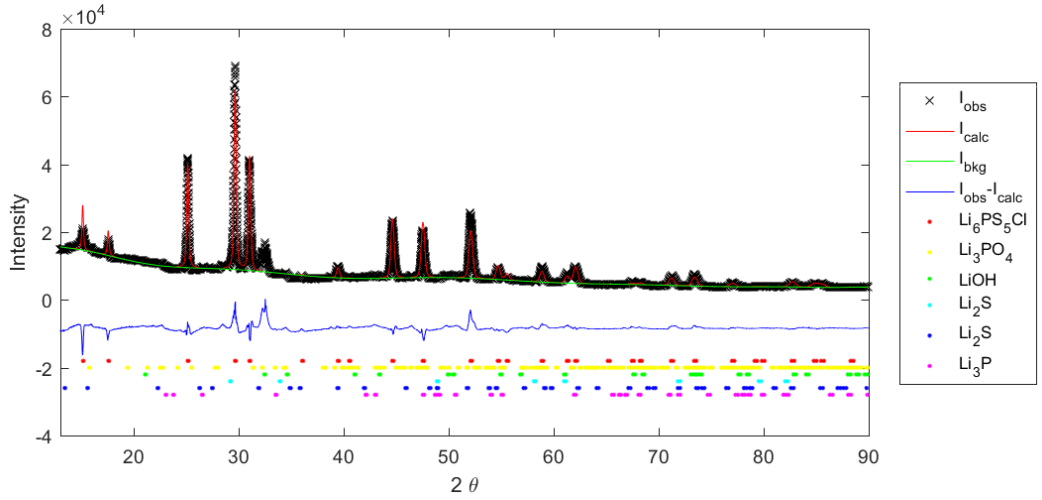

Figure 3.7: Ex-situ XRD measurement of Li_6PS_5Cl after cycling in a Lithium vs. Indium cell for 100 cycles of 0.2mAh at 30uA.

3.3.2 Ex-situ NMR

Several batteries were measured with ex-situ NMR, which will be referred to as follows:

- Battery 1: cycled at 10uA for 50 cycles
- Battery 1: cycled at 20uA for 50 cycles
- Battery 3: cycled at 30uA for 100 cycles

For most batteries, the Isotopes ^{6}Li, ^{7}Li and ^{31}P were measured. Only the ^{6}Li Lithium spectra are shown because no major difference was detected. ^{7}Li spectras are more sensitive because of the higher natural abundance, but yield broader spectral lines because of the higher quadrupolar moment.

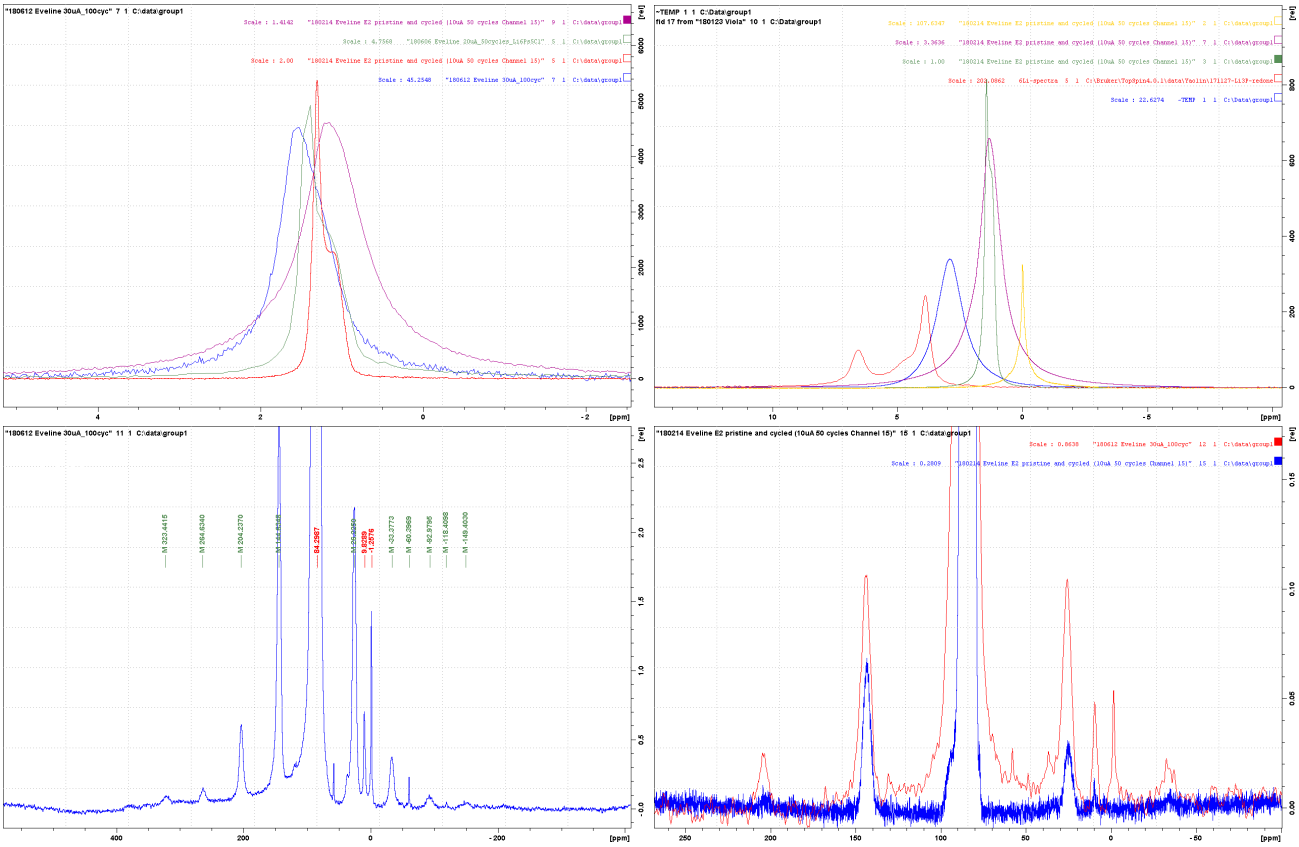

Figure 3.8: Ex-situ NMR measurements. Top left: ^{6}Li NMR of the pristine electrolyte (red), battery 1 (purple), battery 2 (green) and battery 3 (blue). Top right: ^{6}Li NMR spectra of the pristine argyrodite (green),battery 2 (purple), Li_2S (blue), Li_3P (red) and LiCl (yellow). Bottom left: ^{31}P spectra of the argyrodite. All peaks except the three red marked peaks were identified as spinning sidebands. Bottom right: Zoomed in ^{31}P spectra of the pristine electrolyte (blue) and battery 3.

In Figure 3.2 (top-left) the ^{6}Li spectras of the measurements of the three batteries and the pristine electrolyte are shown. The Figure clearly shows that the peaks become broader after cycling compared to before. The Batteries 2 and 3 have a peak that is shifted to the left, whereas the peak of battery 1 is shifted to the right. For battery 2, the second peak is still pronounced as a shoulder, for battery 3 not anymore.

In Figure 3.2 (top left), the ^{6}Li chemical shift of the in literature proposed decomposition products Li_3P (red), Li_2S (blue) and LiCl (yellow) are shown. The chemical shifts of the decomposition products are shifted between 1 ppm to the right (LiCl) and 3-5 ppm to the left (Li_3P) of the Argyrodite peaks.
In Figure 3.2 (top left), the ^{31}P spectra of battery 3 is shown. Three phosphorous peaks were detected: 84.3 ppm, 9.8 ppm, 1.3 ppm. Compared to the pristine electrolyte, the main peak at 84.3 ppm became broader, the intensity of the peak at 9.8 ppm is higher, and the peak at 1.3 ppm is new.

The chemical shift of ^{31}P in Li_3PO_4 has been reported at -10 ppm vs. phosphoric acid (3.5-4 kHz spinning speed) [22] at a magnetic field strength of 7 Tesla. In combination with the XRD measurements and because the peak is already present in the pristine electrolyte, it is very plausible that the peak at 9.8 ppm stems from Li_3PO_4 and that the referenced spectra is off by 0.2 ppm because of the lower resolution.
The chemical shift of ^{6}Li LiOH has been reported as 1.3 ppm vs. LiCl (at 11100 Hz spinning speed) [35], which would overlap with the peak from the argyrodite and does not exclude reaction with water.
The additional peak at 1.3 ppm does not match the ^{31}P resonance of Li_3P (see Annex, Figure 6.3). It can also be excluded that the additional environment at 1.3 ppm belongs to following compounds from the Li_2S-P_2S_5 system: P_2S_5, $LiPS_3$, $Li_4P_2S_6$, Li_3PS_4 and Li_7PS_6, as reported ^{31}P chemical shifts are very far away [10]. Also amorphous $(Li_2S)_x - (P_2S_5)_{1-x}$ for x = 0.4, 0.5, 0.6, 0.66 and 0.7 were measured and had a chemical shifts between 83-89.8 ppm and can also be excluded [10].
In table 3.1, the Spin-lattice relaxation times T1 are given for the measured isotopes and electrolytes. For ^{6}Li, the relaxation time of the pristine electrolyte is about 2 seconds higher compared to the cycled one. For ^{7}Li, relaxation is much faster than for ^{6}Li and the pristine electrolyte has about 26ms longer relaxation time. For ^{31}P, the relaxation time was 2 seconds faster for the cycled electrolyte compared to the pristine one.

Table 3.1: T1 measurements of Li_6PS_5Cl

Isotope	Pristine (p)/cycled (c)	T1
^{6}Li	c	3.158s
^{6}Li	p	5.029s
^{7}Li	c	226.3ms
^{7}Li	p	252.6 ms
^{31}P	c	7.627s
^{31}P	p	5.609s

3.4 Neutron depth profiling

3.4.1 NDP Cell development

In this section, the development of a solid-state cell that can be used within the neutron depth profiling setup is documented. First, the design considerations used for the cell development are discussed. Then, the electrochemical performance of the design is tested under different circumstances.

Design considerations

Both for the electrochemical performance as well as for the measurement setup, the battery assembly has to follow certain criteria. Due to the high reactivity of most materials used, materials that lead to side reactions have to be avoided. Due to the same reason, the assembly should be airtight to avoid side reactions with air or water vapor. For the basic function of the battery an electrically insulating case has to separate the anode from the cathode. There should be good electrical contact between the current collector and the electrodes. Out of practical reasons, the assembly should work for different chemistries, so the volume of the battery should be adjustable and the current collectors easily exchangeable. As the cell should be used within the NDP setup, some additional requirements hold:

- The Tritons have a maximum range of about 40 um. Therefore, a window needs to be assembled on the battery that encapsulates the battery, is airtight and which should have low stopping power in the energy range of the tritons of interest.
- The assembly should consist of materials that either do not activate by neutrons, or have a very short half life, as radiation should always be kept as low as reasonably achievable. Furthermore, a short half live ensures quick cool down and a background contribution proportional to the neutron beam.
- For high and homogeneous neutron intensity, the material of the case should have a low scattering and absorption cross section.
- The cell can ideally be used for ex-situ, in-situ and operando measurements

As the regular solid-state cells work very well and to ensure correlation between the phenomena observed in those cells and the NDP-cell, the regular solid-state cell design was taken as a starting point. The following parts were modified to reach the requirements of the NDP setup (see Figure3.9):

- All stainless steel parts were replaced by Aluminum parts, which is a standard material for measurement setups with neutron radiation because of the low scattering and absorption cross sections. The final design may also be made from titanium, which has a higher scattering cross section and higher cost, but which does not activate and is mechanically stronger, so the case can be made smaller.
- On one side, the current collector was removed and replaced with the window. Due to the function as current collector, the window should be electrically conducting.
- To ensure flexibility in height and good electrical contact with the current collector, a spring was placed opposite to the window.
- To allow for different chemistries, the current collector on both sides can be exchanged easily by selecting another window material or replacing the titanium disk.

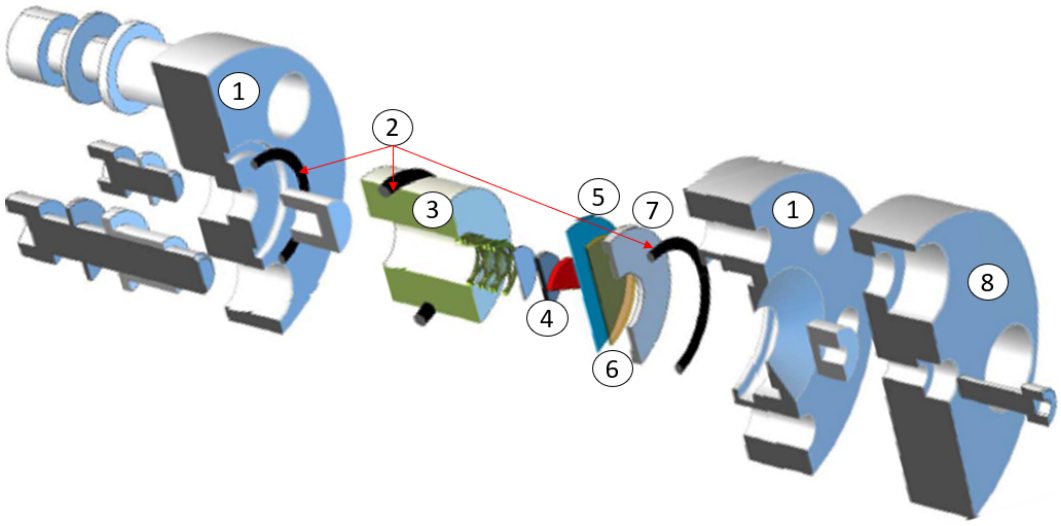

Figure 3.9: NDP cell design: 1) Aluminum casing 2) O-rings 3) Insulating aluminum oxide ring 4) stack with spring, titanium current collector and the battery 5) titanium foil for window 6) Collimator plate (future) 7) titanium spacer to protect the window from the O-ring 8) removable negative for cycling / in-situ measurements.

- O-rings were placed at all intersections for sealing.
- In the second iteration, a removable plug to cover the window was added, for improved contact. In the future, it would be nice to exchange the plug with a collimator disk.

Electrochemical performance of the cell

The cell was assembled as follows. First, the electrolyte pellet was pressed with 10MPa in a pellet press. It was then taken out and placed inside the Aluminum Oxide ring. The foil was placed below the Aluminum oxide ring and the lithium metal electrode and a titanium current collector was put on the other side. This was pressed with 2MPa and put inside the battery assembly. The spring was put on the titanium current collector and the battery was closed.
The assembly without the removable plug was tested with different foils as windows and the results are shown in Figure 3.10. Already for the first plating cycle, RVS (rust-free steel), Indium and Aluminum windows showed very large voltage drops due to loss of contact with the window/current collector. Therefore, Lithium metal was rolled out as thin as possible (around 40um) and put on a steel window. The Lithium significantly increased the cycling performance of the cell, probably because the soft Lithium metal was partially pressed inside the electrolyte. However, as the NDP probing depth is limited, the lithium metal layer would have to be very thin due to the limited probing depth pf the NDP.
Attempts at making such thin Lithium metal foils by rolling it out mechanically and melting it were made. However, the desired thickness and homogeneity could not be achieved with those processes. In the scope of this thesis, it was not possible to get it from external partners.
The effect of pressure on the window was on the cycling performance was investigated. This was first tested by making the same cell without a window, and then by making an in-situ cell with removable plug for the window. The cell was cycled at 30uA, a plating capacity of 0.2mAh and a cutoff voltage of 1V during stripping (Figure 3.11). The plating voltage is similar to the voltage obtained with the regular solid-state cells, and the voltage stays constant during the break. Also the stripping voltage is comparable to the cells. After stripping the voltage

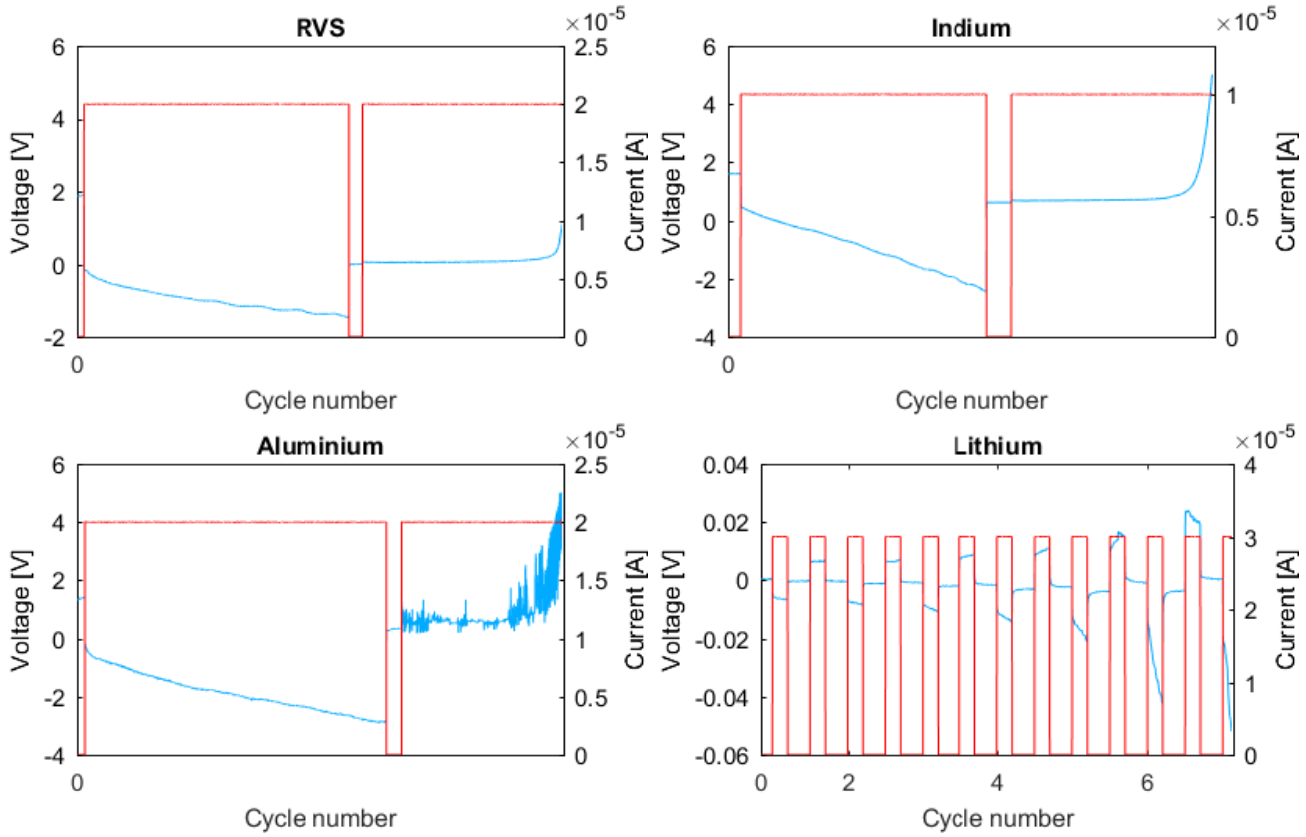

Figure 3.10: Electrochemical performance of the first iteration of the NDP cell without removable plug. Red line corresponds to the current, blue to the voltage. Different window materials were tested to investigate the electrical contact.

clearly drops during the breaks, which indicates that the large volume decrease still leads to contact problems. The reversibly cycled capacity varies a bit more, but is slightly higher.

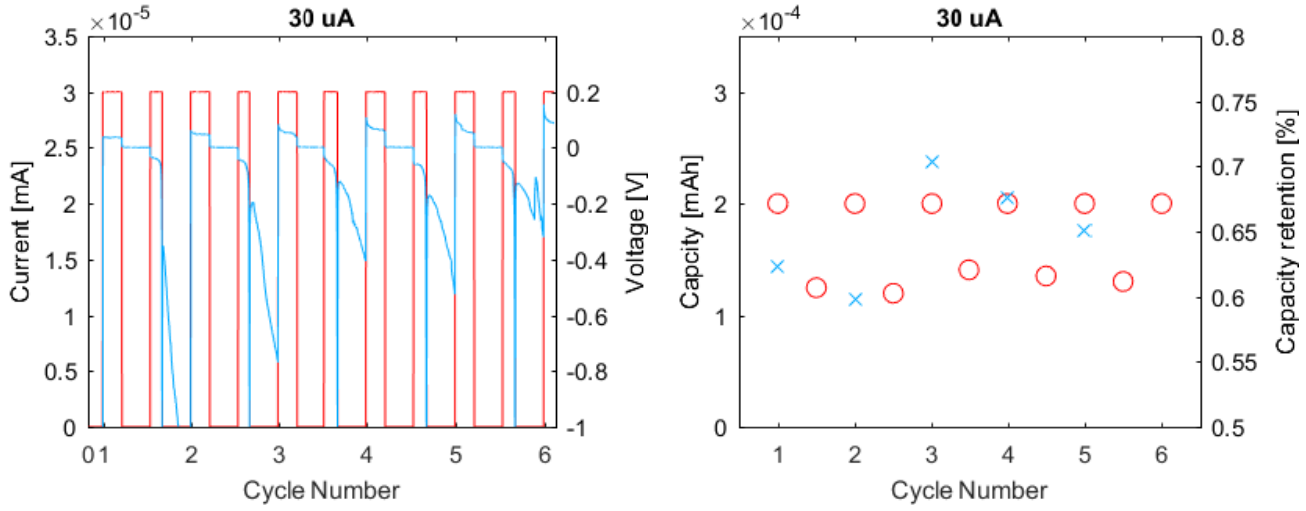

Figure 3.11: Electrochemical performance of the NDP cell for Lithium plating on titanium with removable plug attached to the window. Red corresponds to the current (left) and plated capacity [mAh] (right), blue to the voltage (left) and capacity retention [%] (right)

3.4.2 NDP data analysis

The output of an NDP measurements are the amount of counts within a specific energy range. As described in section 1.2.1, there are different ways to analyze the spectra. Here, first the stopping powers of different materials relevant for the system are analyzed and some approximations are discussed. Then, different electrolyte layer thicknesses were simulated with TRIM and the effect of energy straggling is investigated. Finally, the Energy versus depth relationship obtained with SRIM and TRIM are compared.

SRIM

The stopping Power was calculated for different components of the system using the SRIM stopping power calculator, the results can be seen in Figure 3.12. The stopping power is largest for the metal windows, higher for copper compared to titanium. The large difference between the two metals in the energy region between 1000 and 2000 keV indicates, that quite a lot of energy can be saved by choosing a suitable metal window. For an electrically conducting electrode, it could be attempted to make the electrical contact straight on the electrode and using a non-metal window.
The stopping power of air is very low compared to the solids, but due to the large distance between the window and the detector it can not be neglected.
According to Bragg's rule, the stopping power for compounds is the added stopping power of the individual elements. The Figure shows that the stopping power of the Li_2S, Li_3P and LiCl are slightly higher than Li_6PS_5Cl and Lithium metal. This finding is inconsistent with what would be predicted by Bragg's rule, but the reason therefore is that for the decomposition product, the theoretical density resulting from the atomic weights and the lattice parameter was used, whereas for the electrolyte the pellet density was measured experimentally.

Again applying Bragg's rule, the stopping power only changes with the amount of Lithium that is plated during the operation of the battery. Assuming homogeneous plating, the thickness of the plated Lithium metal s can be estimated as follows:

$$s[cm] = \frac{3600 C M_{Li}}{q N_a d * A} \tag{3.1}$$

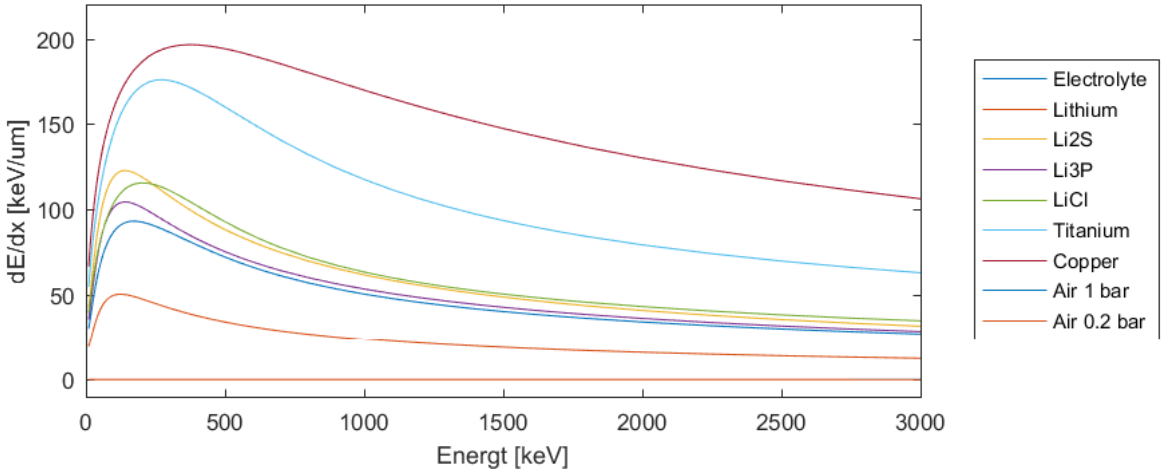

Figure 3.12: Stopping Power of different materials

Where C is the capacity in Ah, M_{Li} the molar mass of Lithium, q the elemental charge, N_a the Avogadro number, d the density and A the area on which is plated. Using this formula and assuming a density of 0.534 g/cm^3, the 0.2 mAh that are plated correspond to 1.23 um lithium metal. Depending on the energy of the tritons, this can lead to an additional energy loss of around 50 keV (see Figure 3.12). If the capacity retention is not equal to one, the stopping power also increases for consequent cycles.
When investigating the titanium foils by eye after failure, rings were detected on the titanium foil, which disappeared after rinsing them with water by reacting to a gas that smelled like hydrogen. Therefore, it can be assumed that the Li-metal does not form a homogeneous layer, put plates on point-contact positions. Correcting the data analysis for the plated lithium thickness would therefore not necessarily improve the accuracy and the aspect was neglected.

TRIM

To calculate the energy versus depth profile with TRIM, first the system had to be simulated for different material layers. The following layers were simulated:

- Air at 0.2 bars, 3cm
- Air + titanium, 1-10 um with steps of 1 micron
- Air + titanium + electrolyte 1-33 um, with steps of 2 micron

To check whether the Energy distribution of the transmitted particles can be described as Gaussian, histograms were plotted and fitted (see Annex Figure 6.4). For particles that traveled far, gaussians manage to make a perfect fit. For particles that traveled less far, there are a more particles just around the mean.
For each simulation, the mean particle energy was calculated and plotted versus the depth into the electrolyte. The result is shown in Figure 3.13. To estimate the error made because of energy straggling, a model for the energy versus depth relation was made. It was then calculated, what error would be made in terms of the depth, if the energy deviates by 1, 2 or three standard deviations from the mean energy. The standard deviations were found to be within 30-60 keV, which is higher than the typical standard deviation resulting from detector energy

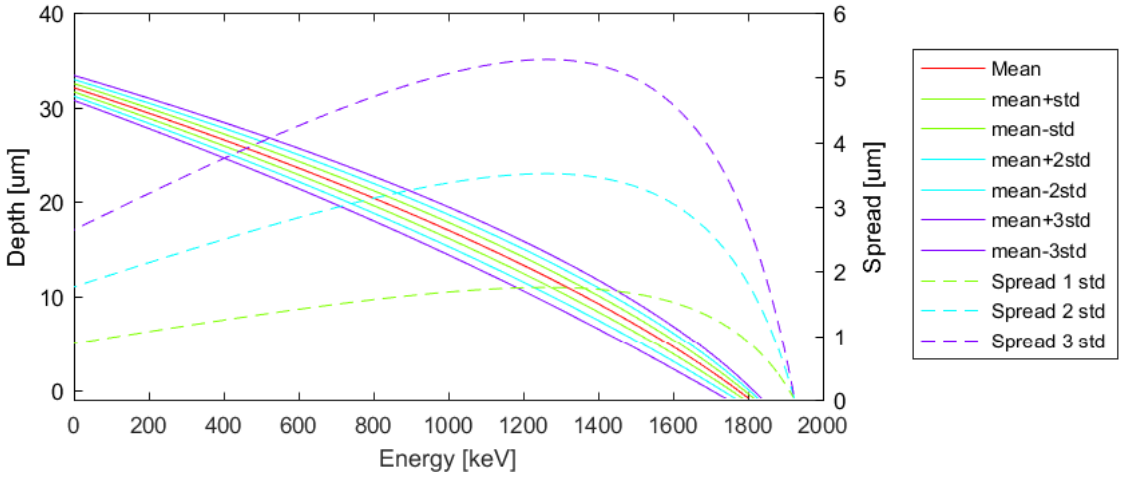

Figure 3.13: The energy versus depth profile obtained with TRIM. The standard deviations is the standard deviation of the triton energy after transmission. The corresponding depth was calculated according to the mean model.

broadening, which is around 20keV [32]. As a property of gaussian distributions, 68.2 % of the data points lie within one standard deviation, 95.4% within 2 and 99.6% within 3.
From this, the spread in depth was calculated. The result shows that 68.2 % lie approximately within 1um, 95.4% within 2 and 3um and 99.5 % within 3-5 um, depending on the residual energy of tritons.

SRIM and TRIM: Comparison

In Figure 3.14, the Energy - depth relationship as obtained from TRIM and SRIM is compared for a system of 10 um titanium and 30um electrolyte. Inside the electrolyte, the profile obtained with SRIM is very close to the median of the transmitted Energy form TRIM for the first 20 um. After that, the energy of the SRIM profile starts to deviate from the median line upwards until it reaches the 0.975 quantile at 40 um.
Surprisingly, a discontinuity at the titanium-electrolyte interface was found for the depth profile using TRIM. The jump in energy is around 200 keV, and deviates from the SRIM profile by about as much. Physically, this does not make sense and the reason for this behavior was not investigated further, as the profile inside the electrolyte is of good agreement between the two methods.

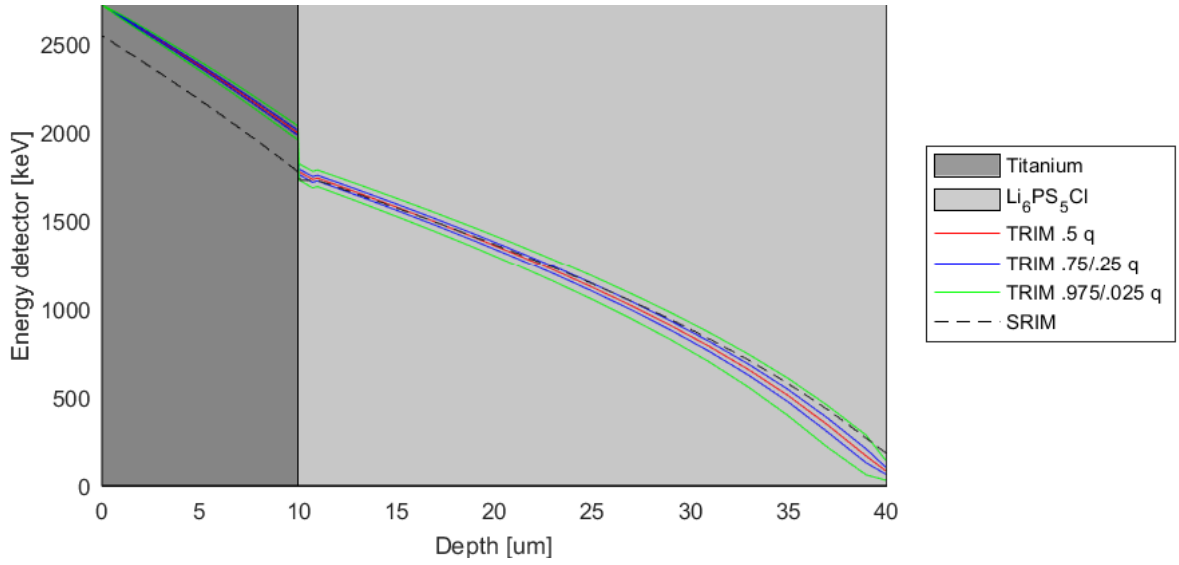

Figure 3.14: Comparison between the data analysis TRIM and SRIM

3.4.3 NDP measurements

Using the cell developed within this thesis, initial NDP measurements were conducted.
In Figure 3.15, the spectra of 0.2 mAh Lithium plated on titanium, the background (which consisted of the cell assembly, the titanium window and the electrolyte pellet) and the plated system with the background subtracted are shown as obtained. The vertical lines correspond to the initial triton energy (2727 keV), the residual energy of the triton when it comes from the interface between the titanium and the electrolyte (1770.5 keV) and the residual energy of a triton arising from 20um into the electrolyte (768 keV). Due to the low amount of counts at lower energies this was selected as the cutoff energy. In the energy range above 2000 keV, there are two peaks that are visible in both spectras.
The energy of the peaks is very close, but slightly too high to correspond to the initial energy of the α particles (2055 keV) or Tritons (2727 keV) ^{6}Li capture reaction. Also, the peaks from the background measurement and the

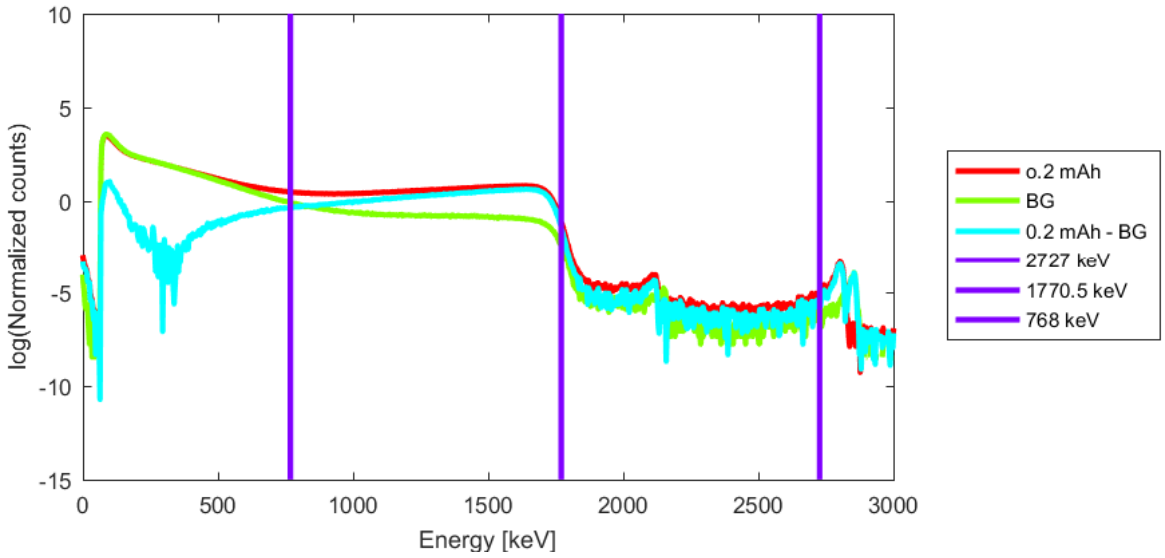

Figure 3.15: NDP spectra obtained for 0.2 mAh plated on titanium foil (red), the background consisting of the setup, cell assembly with electrolyte pellet and titanium window, and the background subtracted signal. The vertical lines correspond to the initial triton energy (2727 keV), the residual energy of the triton when it comes from the interface between the titanium and the electrolyte (1770.5 keV) and the chosen cutoff energy at 20um into the electrolyte (768 keV).

Lithium plated are also slightly shifted from each other.
In Figure 3.16 (left) the same spectra is shown as a function of depth up to 20um into the electrolyte. The ^{6}Li concentration starts rising right behind the titanium foil with a slope of about 0.4 Counts/um.
On the right, the same plot is shown again with error-bars The vertical error bars show the error due to the

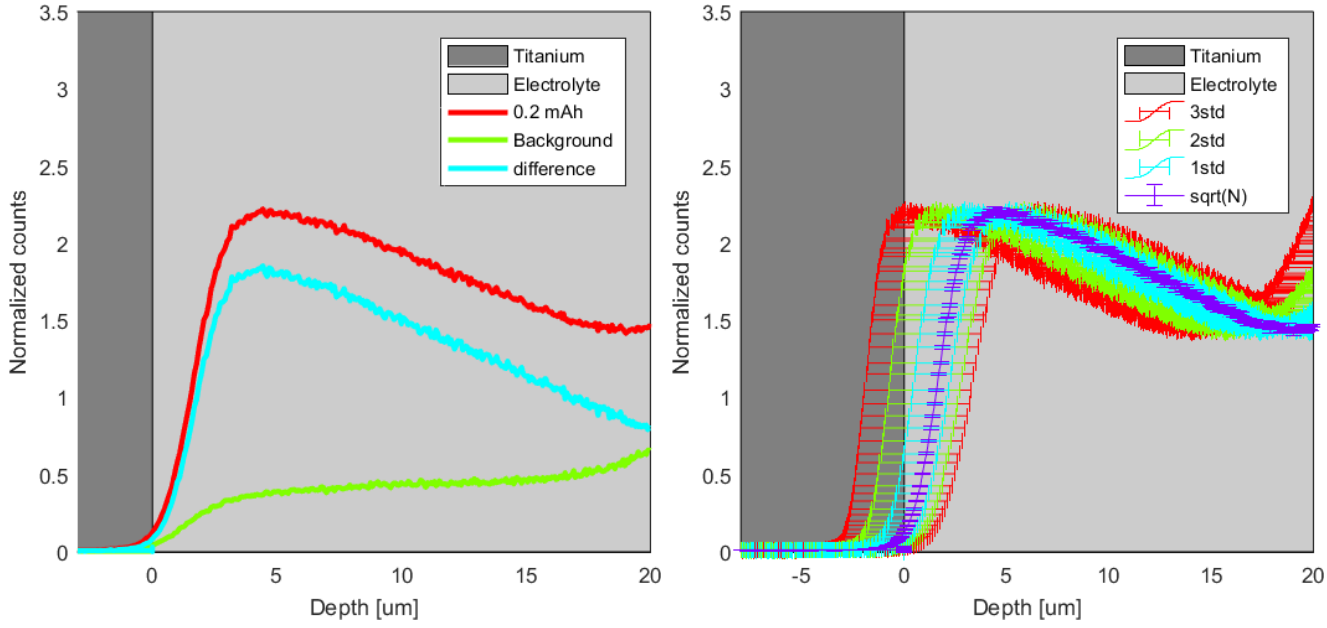

Figure 3.16: NDP spectra of 0.2 mAh plated on 10um titanium foil. On the left, the measured spectra, the background measurement and the background subtracted spectra is shown. On the right, the measured spectra is shown with the errors because of energy straggling (horizontal bars) and the counting errors (vertical bars).

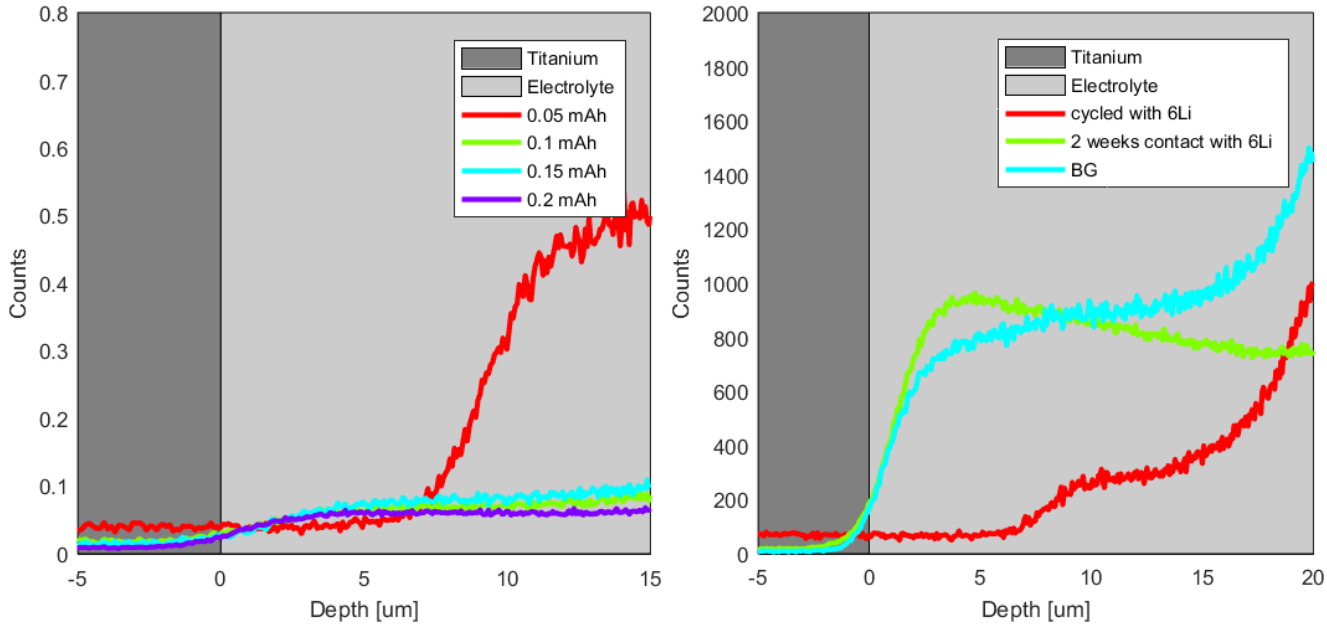

Figure 3.17: Left: NDP In-situ measurements during 4 stages of plating. Right: NDP spectra of pure electrolyte with different ^{6}Li treatments

counting statistics, which in this case is very low as the measurement was made during one hour. For operando measurements, shorter measurement intervals would have to be chosen for a higher time resolution, the error would then become more prominent.
The horizontal error bars indicate the uncertainty in depth because of energy straggling, or more precise, assuming that the measured particle had the mean transmission energy of it's corresponding depth, the error bar indicates the depth the same particle would have been assigned to if it's energy deviated from the mean energy of the transmitted particle by one, two or three standard deviations.

To investigate the growth mechanism of Lithium, in-situ measurements were performed. The same battery was measured after plating for 0.05, 0.1, 0.15, and 0.2 mAh Lithium metal (Figure 3.17 (left)). The beam monitor did not work during 3 of the 4 measurements. Therefore, the spectras were normalized to the same measurement time. As the measurements were conducted right after each other, and the neutron beam strength depends on the reactor power which does not deviate much in time, this is a justified approximation. Still, the spectra for 0.05 mAh plated Li-metal shows more counts than the spectras with a higher amount of plotted Li-metal. Also the normalized amount of counts is very low compared to Figure 3.16, and the spectra also does not show the same characteristic profile as in Figure 3.16, which indicates that other problems with the setup may have been present.
In Figure 3.17 (right), ^{6}Li doping experiments were attempted. Therefore, one battery was cycled in a regular all solid-state battery with electrodes with 95% ^{Li} at a current density of 30uA two weeks. Another battery was assembled the same way, but just left to rest for two weeks. The battery then was assembled, the electrolyte hand ground to a powder and a pellet for NDP was made.
Unfortunately, also here the beam monitor did not work and all the measurements were normalized to the same measurement time. There are more counts for the electrolyte that was in contact with the ^{6}Li between 2-5 um into the material, but less counts at higher depths. The cycled electrolyte shows even less counts. Considering the

same electrolyte was used and the pellet was made the same way, the minimum amount of counts that should have been counted are the background counts. As this is not the case, also here, other problems with the setup may have been present.

4. Discussion

Electrolyte characterization

The electrolyte was characterized with XRD, NMR and TEM with EDX. The XRD measurements indicate pure phased Li_6PS_5Cl. However, measurements of the same electrolyte batch showed quite large differences in relative intensity and the Rietfield refinements proved difficult. Reasons therefore may be:

- Low contrast between Cl and S and the low sensitivity of Li when using x-rays (also stated in [9]).
- The high reactivity of the argyrodite even in the airtight sample holder leading to a gradient in peak intensity during one scan because reactions on the surface may enhance/reduce the signal.
- Differences in crystallite size leading to apparent preferred orientation. This phenomena could be enhanced because the sample, unlike non-air-sensitive samples, can not be spun during the measurement, which leads to the same area being in the focus of the beam.
- Contributions because of dust/powders sticking to the surface of the Kapton cover on the sample holder, which is difficult to clean and dry. Other factors leading to complex background functions.

When considering the results from the diffraction data, the fact that two lithium environments are detected with NMR is surprising, as there is only one Wyckhoff site for Lithium atoms and the area under the curve is too large for an impurity phase. There are several reasons that could explain the appearance of the second peak:

- Introduction of a second environment because of the different shielding of the Chloride dopant compared to the Sulfur atoms.
- Differences in the chemical shift for Li-atoms in the bulk or on the surface of the particles.
- Incomplete reaction leading to another compound in amorphous form or with diffraction peaks that overlap with the argyrodite and which therefore can't be detected by diffraction methods.

Also the EDX spectra of the particles with TEM showed one particle that was partially depleted of Cl, because of unknown reasons. As only two particles were studied, it is not known whether the inhomogeneous Cl- distribution is a common feature or an exception. Therefore, it would be interesting to study more particles.
The combination of the second Li-environment found with NMR and the EDX measurements do not exclude that the phase transformation was not complete, even though with XRD the material appears pure-phase.

Electrochemical performance of the batteries

Lithium indium, symmetric Li-Li and lithium-titanium cells were prepared and cycled.
Many Li-In cells reached 50 cycles and one cell reaching 100 cycles at different current densities. 100% capacity retention was obtained for all cells, which means that the indium side exhibited perfectly reversible cycling.
The overpotential increased with the amount of cycles. The increase of the overpotential can arise from both a decrease in bulk conductivity, and a growing resistive interphase. It would be interesting to investigate this with AC-impedance measurements.
The overpotential also increased when going from 10 to 30uA, and then decreased for higher current densities, where also dynamic short-circuits started to be observed. The overpotential of the batteries cycled at 60 and 70 uA was again larger, but not quite as large as for 30uA. It is possible that the dynamic short-circuit condition and the lower overpotenital are related. If the increase in overpotential over time stems from forming a resistive interphase, the interphase cracks, which would lead to a freshly exposed surface. However, as the trend is not clear, no conclusions can be drawn.
To learn about the cycling performance that could be expected from the NDP cell, Lithium was plated on titanium in the regular solid-state cells. The capacity retention was relatively low, between 60 and 70 %, and the batteries failed much faster than the symmetric Li-Li cells. In [36] it was proposed that contact problems at the electrodes can lead to the acceleration of dendritic growth, which can be considered as a reason why different values for limiting currents in similar cells are reported in literature. This could be the reason for faster short-circuiting of the lithium-titanium cell.

Although not shown in the result section, but the electrochemical performance of the batteries improved significantly when a new cell assembly design was adapted half way into this thesis. This emphasizes the importance of a good cell assembly design. Even with the new cell design, however, the reproducibility of the results was difficult. Many cells were assembled, some failed from the start, others were found to leak, some cells failed suddenly and there was a large variation in the performance of the batteries. This indicates that the cell design is not yet robust enough, or that the process control during the assembly or the environmental conditions during cycling need to be improved. Additionally, the initial cell was difficult to disassemble. This can also lead to problems for ex-situ measurements.

Ex-situ measurements

To study the stability of the interface between Li-metal and Li_6PS_5Cl, ex-situ measurements of the cycled electrolyte were conducted.

With ex-situ XRD, no additional phases could be identified after cycling, except for impurities that formed due to the reaction with water. This indicates that no other crystalline compounds were present. However, maybe the surface to bulk ratio was too low, and the decomposition products are there but not on the surface of the sample. Therefore, it would be interesting to try with neutron diffraction, due to the higher penetration depth and larger sample volume. With neutron diffraction it would also be interesting to investigate whether changes in the Li-sub-lattice occur upon cycling.
The ex-situ Li-NMR spectras showed peak broadening of the Li-peaks after cycling, but no clear novel peaks were detected. It would be interesting to investigate whether the peak broadening arises from signal overlap

with decomposition products or because of a change in Li-ion mobility.
For ^{31}P NMR, a peak was found which can most probably be assigned to Li_3PO_4. It would be interesting to measure Li_3PO_4 to confirm this on the same NMR machine.
Another additional peak was found at 1.3 ppm. It could be excluded since the resonance belongs to Li_3P and many other compounds in the Li_2S-P_2S_5 system, but the environment could not be identified.

The above findings indicate that the electrolyte is kinetically quite stable for the investigated Li-Indium cells. None of the decomposition products identified in the literature could be confirmed. DFT simulations have shown highly favorable decomposition [6, 45]. Relatively good stability has been reported before [44], which can be confirmed by the results from this thesis. It is possible that the apparent stability stems from sluggish kinetics of the decomposition reaction.

NDP cell development

A NDP-cell was designed, implemented and tested. The results of the electrochemical measurements were comparable to the measurements conducted with the regular solid electrolyte cells, except for a voltage drop during the break after stripping, because of loss of contact. The contact was slightly improved with a removable plug for in-situ measurements, and significantly improved by turning the cell into a symmetric Li-Li cell by adding a thin layer of Li-metal between the window and the pellet.
With the processes available, it was not possible to fabricate Li-metal thin enough to see something with NDP. It also could not be sourced from external partners. If it were available, it would also be interesting to replace the titanium window with another material with lower stopping power, such as Kapton, as the Lithium layer could simultaneously be used as a current collector.
It would also be interesting to replace the removable plug with a collimator plate which can be put below the window. Since it would exert additional pressure, as well as let the signal pass through, it would be a good step to progress fro m in-situ to operando measurements.
For the design of the collimator, the thickness of the plate and size of the holes would have to be optimized smartly, as it has a strong influence on the achievable depth resolution of the measurement. However, there is also a trade-off between the resolution and the signal intensity, which is important when considering operando measurements.
It would further be interesting to test the cell for batteries with different electrodes. If the electrodes could be coated straight onto the window, or if the electrical contact could be made by sputtering a metal layer on the electrode/electrolyte pellet, the electrochemical performance may also improve.

NDP Data analysis

Literature about the NDP data analysis was studied and the standard method was implemented. The standard data analysis method does not take into account the effect of geometrical depth resolution, detector energy broadening and energy straggling.
To investigate the accuracy of the standard data analysis method, the effect of energy straggling was investigated. Therefore, the system was simulated for different thicknesses, and the effect of the deviation of the mean transmission energy on the depth profile was investigated.
The results showed that the effect of energy straggling on the interpretation of the depth profile can be in the range

of several microns and should therefore not be neglected, especially when high (changes in) ^{6}Li concentrations are looked at, as this would lead to many counts in the tails of the probability distribution. In terms of energy, the standard deviation of the broadening function was between 30-60 keV, which is larger than the standard deviation of the detector broadening function reported in literature [32].
The total gaussian broadening of the system has to be calculated according to equation 1.23. The contributions of the detector broadening and energy straggling are combined which would lead to an even larger broadening effect.
Due to the large influence of above named aspect, the deconvolution of the system should be done with the response function specified in equation 1.22. Therefore, the different algorithmic approaches already developed in literature could serve as a starting point.
The effect of the setup geometry on the resolution of the measurements has not been investigated in the scope of this thesis, but it should be included as well.
Assuming Bragg's rule applies, the stopping power of the material is directly proportional to the the amount of atoms of a certain element. Therefore, cycling the battery will affect the stopping power, especially when cycling large capacities or if Li-accumulation is observed. Due to inhomogeneous plating, this was neglected in the scope of this thesis. However, it was estimated that 0.2mAh of Li-atoms may change the energy up to 50keV, and should therefore not be neglected for more homogeneous Li- distributions.

NDP measurements

Several initial NDP measurements were made. First of all, the background signal coming from the cell setup, the cell assembly, and the electrolyte pellet behind the titanium window was measured. Then, a measurement with 0.2mAh lithium plated on titanium foil was conducted. Further, a series of in-situ measurements, where 0.05, 0.1, 0.15, and 0.2 mAh were plated, was attempted. The effect of cycling the electrolyte with 95% ^{6}Li and leaving the pellet in contact with it, was investigated.

Several problems with the setup were faced. Firstly, the beam monitor did not work for several measurements. In that case, the measurements were normalized to the same total measurement time. Then, peaks in the spectra which most probably correspond to the energy of the tritons and alpha particles were found at an energy that is too high. Two different spectra, which were measured with a longer break in between, also showed a shift of those peaks. Also for the initial measurement, the rise in the amount of Li-ion counts starts deeper into the electrolyte than one would expect.
As this phenomena is seen across most measurements, and since the initial energy of the tritons and alpha particles is well defined, it can be assumed that this arises from the energy calibration of the detector. Another reason could be that as there are many counts registered in the low energy segment, the probability of a low energy particle reaching the detector at the same time as a high energy particle is not negligible. The two particles would then be registered as one with the sum of the energy of both. This could lead to a shift in the energy spectra. As the entire peak is shifted, however, this is not very plausible. The relative shift between the two spectra may also arise from a variation in air-density inside the chamber, which influences the stopping power.

In-situ measurements as well as doping experiments were attempted. The spectra measured do not show what would be expected considering the initial plated and background spectra. One reason could be that there was no holder for the cell, so the alignment of the cell with the beam and the detector had to be made by hand. If the

battery is slightly too far back, then the neutron may miss a larger part of the pellet, leading to less counts in the low energy spectrum. If the angle is not perfect, then there will be a larger distance the particles have to travel through the titanium, also leading to a shift in the spectrum along the depth. However, many measurements barely had any counts in the high energy spectra. The alignment would have to be extremely bad for this to happen.

If the reason for the weird measurements were issues with the electrochemical operation of the cell, one would at least expect to measure the same amount of counts as for the background contribution, which was not the case. Therefore, it can not be excluded that there were other issues present and no conclusions can be drawn about fundamental electrochemical aspects.

5. Conclusions and Recommendations

The electrolyte characterization left some doubts about whether the electrolyte phase transition is complete, due to an inhomogeneous Cl distribution found with EDX (TEM) and two Li-environments found with NMR. It would be interesting to study more EDX profiles, and to understand why two lithium environments are present. Due to the difficulties faced with the XRD measurements, XRD may not be the ideal method to check phase-purity.

The electrochemical performance of the different batteries was quite good but not very consistent, and the influence of the cell and the way it was assembled is quite large, which also showed in the difficulty to reproduce results. Also for example the increase-decrease-increase in overpotential observed when increasing the current density, leaves open questions.

It would be interesting to determine what cell aspects and processes during the assembly can lead to changes in overpotential or preliminary failure. This could help to improve the process control which is important if, for example, studies with a variety of cells are performed to study the effect of different operating conditions.

It was not possible to confirm the decomposition products suggested in literature with ex-situ XRD and NMR. With NMR, significant peak broadening was observed, as well as a new phosphorous environment, which has not been identified. It would be interesting to study the exact origin of the peak broadening, and the new phosphorous environment.

The developed in-situ NDP-cell worked comparably to the regular solid-state cells, with the exception of voltage drops due to loss of contact during breaks after stripping. Significant improvements can be made by adding a thin sheet of Li-metal between the window and the electrolyte pellet. To go towards operando, the removable plug should be replaced by a collimator plate, which would allow a certain pressure on the cell as well as signal transmission. The collimator plate may also improve the geometrical resolution of the setup when designed well. However therefore it also needs to be considered that there is a trade-off between the geometrical resolution and the signal intensity. With the current standard data analysis method, where no energy broadening effects are considered, the depth resolution of the measurements is very low. To reach better spatial resolution, several steps should be taken.

First, NDP spectra should be simulated for different possible concentration profiles and response functions, to learn about the effect of specific aspects on the obtained spectra.

Then, the different deconvolution methods already developed in literature should be studied, implemented, and it should be investigated whether they are suitable for the concentration profiles that can be expected for measurements with batteries. The deconvolution methods should also be tested on the simulated spectras, as it allows for direct comparison.

Due to the possible influence of instrumental aspects, it would also be interesting to make samples with well-defined Li-ion concentration profiles, which can also be used to detect other non-idealities of the setup and to investigate the accuracy of the data analysis on a real spectra.

Bibliography

[1] Jérémie Auvergniot et al. “Interface stability of argyrodite Li6PS5Cl toward LiCoO2, LiNi1/3Co1/3Mn1/3O2, and LiMn2O4 in bulk all-solid-state batteries”. In: *Chemistry of Materials* 29.9 (2017), pp. 3883–3890.

[2] Peng Bai and Martin Z Bazant. “Charge transfer kinetics at the solid–solid interface in porous electrodes”. In: *Nature communications* 5 (2014), p. 3585.

[3] J.P. Biersack and L.G. Haggmark. “A Monte Carlo computer program for the transport of energetic ions in amorphous targets”. In: *Nuclear Instruments and Methods* 174.1 (1980), pp. 257–269.

[4] Sylvain Boulineau et al. “Electrochemical properties of all-solid-state lithium secondary batteries using Li-argyrodite Li6PS5Cl as solid electrolyte”. In: *Solid State Ionics* 242 (2013), pp. 45–48.

[5] Hao Min Chen, Chen Maohua, and Stefan Adams. “Stability and ionic mobility in argyrodite-related lithium-ion solid electrolytes”. In: *Physical Chemistry Chemical Physics* 17.25 (2015), pp. 16494–16506.

[6] Tao Cheng et al. “Quantum Mechanics Reactive Dynamics Study of Solid Li-Electrode/Li6PS5Cl-Electrolyte Interface”. In: *ACS Energy Letters* 2.6 (2017), pp. 1454–1459.

[7] Xin-Bing Cheng et al. “Toward safe lithium metal anode in rechargeable batteries: a review”. In: *Chemical reviews* 117.15 (2017), pp. 10403–10473.

[8] Jang Wook Choi and Doron Aurbach. “Promise and reality of post-lithium-ion batteries with high energy densities”. In: *Nature Reviews Materials* 1.4 (2016).

[9] Hans-Jörg Deiseroth et al. “Li6PS5X: a class of crystalline Li-rich solids with an unusually high Li+ mobility”. In: *Angewandte Chemie International Edition* 47.4 (2008), pp. 755–758.

[10] Hellmut Eckert, Zhengming Zhang, and John H Kennedy. “Structural transformation of non-oxide chalcogenide glasses. The short-range order of lithium sulfide (Li2S)-phosphorus pentasulfide (P2S5) glasses studied by quantitative phosphorus-31, lithium-6, and lithium-7 high-resolution solid-state NMR”. In: *Chemistry of Materials* 2.3 (1990), pp. 273–279.

[11] Jian Gao, Si-Qi Shi, and Hong Li. “Brief overview of electrochemical potential in lithium ion batteries”. In: *Chinese Physics B* 25.1 (2015), p. 018210.

[12] Yuping He and Howard Wang. “In-situ Neutron Techniques for Lithium Ion and Solid-State Rechargeable Batteries”. In: *Handbook of Solid State Batteries*. World Scientific, 2016, pp. 51–77.

[13] J. Jaguemont, L. Boulon, and Y. Dubé. “A comprehensive review of lithium-ion batteries used in hybrid and electric vehicles at cold temperatures”. In: *Applied Energy* 164 (2016), pp. 99–114.

[14] Niek JJ de Klerk, Irek Rosłoń, and Marnix Wagemaker. “Diffusion mechanism of Li argyrodite solid electrolytes for Li-ion batteries and prediction of optimized halogen doping: the effect of Li vacancies, halogens, and halogen disorder”. In: *Chemistry of Materials* 28.21 (2016), pp. 7955–7963.

[15] Allen C Larson and Robert B Von Dreele. "Gsas". In: *Report lAUR* (1994), pp. 86–748.

[16] Zhe Li et al. "A review of lithium deposition in lithium-ion and lithium metal secondary batteries". In: *Journal of Power Sources* 254 (2014), pp. 168–182.

[17] Dingchang Lin, Yayuan Liu, and Yi Cui. "Reviving the lithium metal anode for high-energy batteries". In: *Nature nanotechnology* 12.3 (2017), p. 194.

[18] Helmut Mehrer. *Diffusion in solids: fundamentals, methods, materials, diffusion-controlled processes*. Vol. 155. 2007.

[19] Charles Monroe and John Newman. "Dendrite growth in lithium/polymer systems a propagation model for liquid electrolytes under galvanostatic conditions". In: *Journal of The Electrochemical Society* 150.10 (2003), A1377–A1384.

[20] Charles Monroe and John Newman. "The effect of interfacial deformation on electrodeposition kinetics". In: *Journal of The Electrochemical Society* 151.6 (2004), A880–A886.

[21] Charles Monroe and John Newman. "The impact of elastic deformation on deposition kinetics at lithium/polymer interfaces". In: *Journal of The Electrochemical Society* 152.2 (2005), A396–A404.

[22] I.L. Mudrakovskii et al. "31P nmr study of I–IV group polycrystalline phosphates". In: *Journal of Physics and Chemistry of Solids* 47.4 (1986), pp. 335–339.

[23] Motohiro Nagao et al. "In situ SEM study of a lithium deposition and dissolution mechanism in a bulk-type solid-state cell with a Li2S-P2S5 solid electrolyte". In: *Physical Chemistry Chemical Physics* 15.42 (2013), pp. 18600–18606.

[24] Gholam-Abbas Nazri and Gianfranco Pistoia. *Lithium batteries: science and technology*. Springer Science & Business Media, 2008.

[25] JFM Oudenhoven et al. "In Situ Neutron Depth Profiling: A Powerful Method to Probe Lithium Transport in Micro-Batteries". In: *Advanced Materials* 23.35 (2011), pp. 4103–4106.

[26] Oliver Pecher et al. "Materials' methods: NMR in battery research". In: *Chemistry of Materials* 29.1 (2016), pp. 213–242.

[27] Yaoyu Ren et al. "Direct observation of lithium dendrites inside garnet-type lithium-ion solid electrolyte". In: *Electrochemistry Communications* 57 (2015), pp. 27–30.

[28] M. Safari. "Battery electric vehicles: Looking behind to move forward". In: *Energy Policy* 115 (2018), pp. 54–65.

[29] Atsushi Sakuda et al. "Evaluation of elastic modulus of Li2P2S5 glassy solid electrolyte by ultrasonic sound velocity measurement and compression test". In: *Journal of the Ceramic Society of Japan* 121.1419 (2013), pp. 946–949.

[30] Henry JS Sand. "III. On the concentration at the electrodes in a solution, with special reference to the liberation of hydrogen by electrolysis of a mixture of copper sulphate and sulphuric acid". In: *The London, Edinburgh, and Dublin Philosophical Magazine and Journal of Science* 1.1 (1901), pp. 45–79.

[31] Paul Schanda and Matthias Ernst. "Studying dynamics by magic-angle spinning solid-state NMR spectroscopy: principles and applications to biomolecules". In: *Progress in nuclear magnetic resonance spectroscopy* 96 (2016), pp. 1–46.

[32] JK Shultis et al. "Notes on neutron depth profiling". In: *Engineering Experiment Station Report* 298 (2003).

[33] M. Thackeray, C. Wolverton, and E. Isaacs. "Electrical energy storage for transportation-approaching the limits of and going beyond lithium-ion batteries". In: *Energy Environ. Sci* 5 (7 2012), pp. 7854–7863.

[34] Brian H Toby. "EXPGUI, a graphical user interface for GSAS". In: *Journal of applied crystallography* 34.2 (2001), pp. 210–213.

[35] Chuan Wan et al. "Multinuclear NMR Study of the Solid Electrolyte Interface Formed in Lithium Metal Batteries". In: *ACS applied materials & interfaces* 9.17 (2017), pp. 14741–14748.

[36] Chengwei Wang et al. "In Situ Neutron Depth Profiling of Lithium Metal–Garnet Interfaces for Solid State Batteries". In: *Journal of the American Chemical Society* 139.40 (2017), pp. 14257–14264.

[37] Ziying Wang and Ying Shirley Meng. "Analytical Electron Microscopy — Study of All Solid-State Batteries". In: *Handbook of Solid State Batteries*. 2nd. WORLD SCIENTIFIC, 2015. Chap. Chapter 4, pp. 109–131.

[38] Sebastian Wenzel et al. "Interfacial reactivity and interphase growth of argyrodite solid electrolytes at lithium metal electrodes". In: *Solid State Ionics* (2017).

[39] Chunpeng Yang et al. "Protected Lithium-Metal Anodes in Batteries: From Liquid to Solid". In: *Advanced Materials* (2017).

[40] Chuang Yu et al. "Synthesis, structure and electrochemical performance of the argyrodite Li6PS5Cl solid electrolyte for Li-ion solid state batteries". In: *Electrochimica Acta* 215 (2016), pp. 93–99.

[41] Chuang Yu et al. "Unravelling Li-ion transport from picoseconds to seconds: bulk versus interfaces in an argyrodite Li6PS5Cl–Li2S all-solid-state Li-Ion battery". In: *Journal of the American Chemical Society* 138.35 (2016), pp. 11192–11201.

[42] Seungho Yu et al. "Elastic properties of the solid electrolyte Li7La3Zr2O12 (LLZO)". In: *Chemistry of Materials* 28.1 (2015), pp. 197–206.

[43] Ji-Guang Zhang, Wu Xu, and Wesley A Henderson. "Characterization and Modeling of Lithium Dendrite Growth". In: *Lithium Metal Anodes and Rechargeable Lithium Metal Batteries*. Springer, 2017, pp. 5–43.

[44] Zhixia Zhang et al. "Synthesis and characterization of argyrodite solid electrolytes for all-solid-state Li-ion batteries". In: *Journal of Alloys and Compounds* 747 (2018), pp. 227–235.

[45] Yizhou Zhu, Xingfeng He, and Yifei Mo. "Origin of Outstanding Stability in the Lithium Solid Electrolyte Materials: Insights from Thermodynamic Analyses Based on First-Principles Calculations". In: *ACS Applied Materials & Interfaces* 7.42 (2015), pp. 23685–23693.

[46] James F Ziegler, Matthias D Ziegler, and Jochen P Biersack. *SRIM: the stopping and range of ions in matter*. Cadence Design Systems, 2008.

[47] James F. Ziegler, M.D. Ziegler, and J.P. Biersack. "SRIM – The stopping and range of ions in matter (2010)". In: *Nuclear Instruments and Methods in Physics Research Section B: Beam Interactions with Materials and Atoms* 268.11 (2010). 19th International Conference on Ion Beam Analysis, pp. 1818–1823.

6. Appendix

Table 6.1: Neutron diffraction data: Lattice parameter

Chemical Formula	$Li_{5.95}PS_{4.85}Cl_{1.15}$
Chemical Formula weight	268.56
Lattice parameter a=b=c	9.85555(6)
Cell angle a=b=c	90
Symmetry	cubic
Space group name	F-43 m

Table 6.2: Neutron diffraction data: Unit cell parameter

Atom\Parameter	x	y	z	occup	Thermal disp type	U	Site multip
Li	0.16998	0.16998	0.00746	0.496	Uani	0.10408	48
P	0.5	0.5	0.5	1	Uiso	0.01958	4
S0	0.62205	0.62205	0.62205	1	Uiso	0.02725	16
S1	0	0	0	0.53039	Uiso	0.02141	4
Cl1	0	0	0	0.46961	Uiso	0.02141	4
S2	0.25	0.25	0.25	0.31765	Uiso	0.02742	4
Cl2	0.25	0.25	0.25	0.68235	Uiso	0.02742	4

Figure 6.1: Electrochemical performance of Li-Indium batteries 50uA+

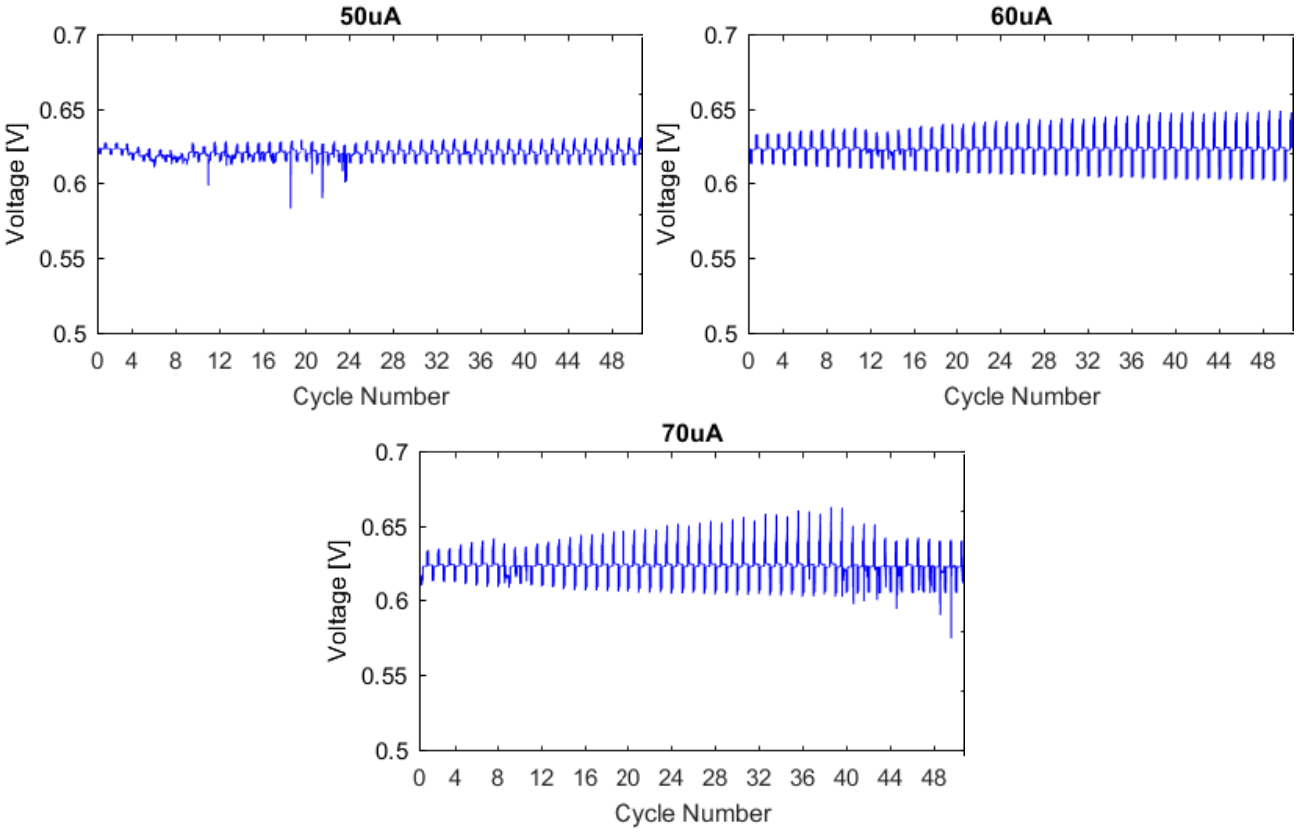

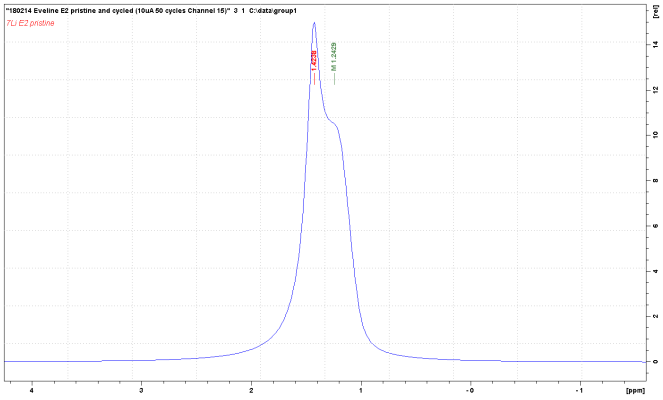

Figure 6.2: ^{7}Li NMR spectra of the pristine electrolyte

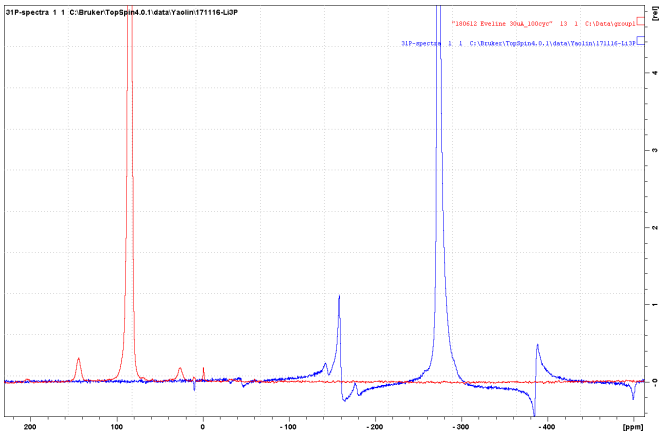

Figure 6.3: ^{31}P NMR spectra of Li_3P and Li_6PS_5Cl

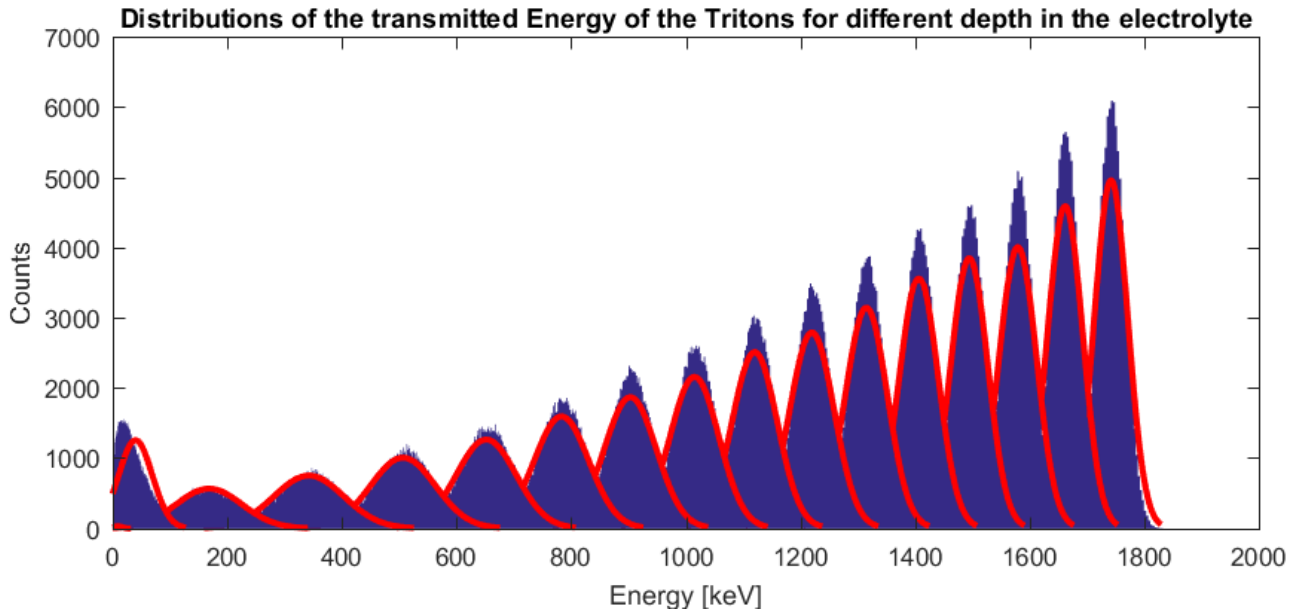

Figure 6.4: Energy distributions of transmitted Tritons for different electrolyte thicknesses. From right to left, the tritons passed through 2 um more than the particle of the previous distribution